

Chapter 2

Microwave Instruments for Observing Tropical Cyclones

Kristina B. Katsaros, Leonid Mitnik and Peter Black

Abstract Development of microwave technologies and our ability to penetrate into Tropical Cyclones (TCs) by instrumented aircraft and observe from satellites have contributed much of the knowledge and understanding that exist today. We can now follow the structure and development of a storm from inception through the many stages towards a dangerous typhoon, hurricane or cyclone, as they are variously called around the globe. The data from satellite microwave radiometers, scatterometers, altimeters, Synthetic Aperture Radars (SARs), microwave sounders, a rain radar and a cloud profiling radar as well as coastal radars, airborne radars and microwave radiometers have all contributed to changing the fields of both TC research and TC operational forecasting.

Keywords Tropical cyclones • Microwave remote sensing • Satellite and aircraft observations

Here we highlight some crucial steps towards current capabilities and describe a short history of these developments and current value of the technology to the field of TC study. We outline the long development of a Stepped-Frequency Microwave Radiometer (SFMR) and the most recent descendant of the same, a scanning microwave radiometer (HIRAD) operated on U.S. research and operational aircraft. These instruments measure surface wind and rain rate inside a storm remotely from safe altitudes. We show the amazing small-scale details of TC structure revealed by SAR's, which have the highest resolution of all satellite microwave instruments. The 30-year development of scatterometry for obtaining

K. B. Katsaros (✉)

Northwest Research Associates, Inc, Bellevue, WA 98052, USA

e-mail: katsaros@whidbey.net

L. Mitnik

V.I. Il'ichev Pacific Oceanological Institute, FEB RAS, Vladivostok, Russian Federation

P. Black

SAIC, Inc. and Naval Research Laboratory, Monterey, CA, USA

surface wind vectors and the multi-faceted evolution of microwave radiometry along with the associated imagers and sounders are reviewed. The use of altimetry to reveal the hidden heat content in subsurface eddies in the ocean, which provide fuel for intensification of TCs, is discussed. The first spaceborne weather radar on the Tropical Rainfall Measuring Mission, that lasted for 10 years, is shown to greatly enhance knowledge of TC structure through its large observational data base of the world's TCs.

This broad review has to be limited to a few salient examples rather than a complete review of each development's history. It concludes with a description of some promising ideas for future advances, such as dual frequency scatterometers, scanning altimeters, scanning SFMRs and a constellation of microwave radiometers with one or more unifying rain radar(s) for inter-calibration between sensors in the Global Precipitation Measuring (GPM) Mission. The latest sensors for salinity measurements may also contribute information about the effects on the upper ocean by the heavy rainfall associated with TC's.

2.1 Introduction

This chapter is focused on observations by microwave remote sensing for research on tropical cyclones, TCs, for use in diagnosing and thereby aid forecasting of tropical cyclones. We will discuss satellite and airborne microwave techniques with both passive and active microwave sensors.

Early work with microwave sensors in space began with try-outs on short space flights and Shuttle missions and many aircraft surveys in the late 1960s and through the 1970s. The possibilities of retrieving sea surface temperature, near-surface winds, total atmospheric water vapor content, total cloud liquid water content, rain intensity and sea ice parameters were documented by Basharinov et al. (1974) in Russia and similar observations were made by U.S. National Aeronautics and Space Administration, NASA (e.g. Nordberg et al. 1969). A certain amount of exchange of information and face to face meetings between the U.S. and the Soviet Union scientists took place in the field of remote sensing even during the cold war days. Figure 2.1 shows many of the pioneers in the field and by its dated look gives a sense of how much time has already passed with access to this technology.

The biggest boost to microwave remote sensing from space came with the dedicated mission, SEASAT, launched in June 1978 by the NASA and enduring for just 3 months (e.g. Jones et al. 1982; Njoku 1982; Katsaros and Brown 1991). The four major techniques that are discussed below were used on this satellite, microwave radiometry (the Scanning Multifrequency Microwave Radiometer, SMMR), scatterometry (the SEASAT scatterometers, SCATT), the SEASAT altimeter (ALT) and the SAR (the SEASAT SAR). The name SEASAT indicates that these sensors give meteorological and oceanographic data over the oceans, while over land the varying emissivity of the background results in signal complexity and often ambiguous interpretation.



Fig. 2.1 Participants of final symposium on the Bering Sea experiment at the A.I. Voeykov Main Geophysical Observatory (MGO), May 1973. *Back row* Dr. W. J. Webster, Leading Engineer M. A. Prokophiev (MGO), Mr. P. Tibido, Prof. W. J. Campbell, Dr. V. V. Melentyev, Head of scientific program onboard MGO Flying Laboratory IL-18, Mr. D. B. Ross, Dr. P. Gloersen, Dr. Yu. I. Rabinovich (MGO), Dr. Yu. I. Loshchilov (AARI), *Second row* Dr. R. O. Ramseier, Dr. E. M. Shul'gina (MGO), Mrs. Gloersen, Dr. E. P. Dombkovskaya (Hydrometcenter USSR), Dr. G. P. Khokhlov (AARI), *Front row* N. Latter (NASA interpreter), Dr. T. T. Wilheit, Dr. L. M. Martsinkevich (NPO Planeta). Photo provided by Prof. Vladimir Melentyev of the NIERSC/St. Petersburg

Radiometry has dominated microwave remote sensing from space with data from another SMMR instrument launched by NASA in 1978 on NIMBUS VII and with the Special Sensor Microwave Imager, SSM/I, in the US Defense Meteorological Satellite Program (DMSP). The first one in a long series of SSM/Is was launched in 1989 (Hollinger et al. 1990). The SEASAT experiment resulted in the original development of algorithms for deriving geophysical variables from the signals. It has jokingly been suggested that it was a blessing that the satellite did not last very long, so that the data collected were thoroughly evaluated for biases and errors. Interpretation in terms of geophysical properties of the atmosphere and the sea required detailed study of the comparison data sets from measurements on or over the ocean. Currently, the heritage instrument, the Special Sensor Microwave Imager Sounder, SSMIS, continues with similar wavelengths as the SSM/I providing images and in addition providing soundings.

Scatterometers only began to be routinely launched in 1991 with the first European Remote Sensing (ERS) satellite and many have followed. SAR's have not been launched routinely by either the European Space Agency (ESA) or the U.S. The best examples of SAR data for tropical cyclone work comes from the

European Envisat and Canadian RADARSAT 1 and 2 in wide swath SAR observations (e.g. Vashon and Katsaros 1999; Horstmann et al. 2005; Mitnik et al. 2005a; Reppucci et al. 2010). Envisat Advanced SAR (ASAR) was launched in 2002. RADARSAT 1 and 2 were launched, respectively in 1995 and 2007, with the objective of observing the Arctic sea ice, but through a special Canadian program, Hurricane Watch (Iris and Burger 2004), has provided excellent high resolution data of TC's, especially in the Caribbean and off the East coast of the USA (e.g. Vachon and Katsaros 1999). More of the background will be recounted in connection with each instrument being discussed.

In Sect. 2.2 we define the instruments that form the basis of our review of TC studies using microwave data. In Sect. 2.3 we give examples of observing TC's with some of the satellite sensors. In Sect. 2.4 emphasis is on practical applications of remote sensing in observing one particular typhoon, named MEGI, which crossed the South China Sea in October 2010. In Sect. 2.5 we summarize the impact of the many microwave instruments on TC research and forecasting and describe a few new instruments in advanced planning stages, a scanning altimeter, a TRMM follow on involving many satellites, and the need for coalitions of agencies to contribute to increased frequency of sampling the important variables. These advances are expected to enhance the value of microwave observations in the near future.

2.2 Instruments

We include here description of the instruments that we refer to in the examples of hurricane studies below to separate the technical details from the scientific use of the data they provide.

2.2.1 *Passive Microwave Radiometry*

Passive microwave sensing of the Earth started in the U.S.S.R. in the early 1960s. The first two satellites to carry four microwave radiometers into space were Kosmos-243 launched in 1968 and Kosmos-384 in 1970. The nadir-viewing trace radiometers operated at wavelengths $\lambda = 8.5, 3.4, 1.35$ and 0.8 cm. The Instantaneous Field Of View (IFOV) was 50×50 km (apogee) and 35×35 km (perigee) at $\lambda = 8.5$ and approximately 22×22 km (apogee) and 15×15 km (perigee) at other wavelengths. The possibilities of retrieving sea surface temperature, near-surface winds, total atmospheric water vapor content, total cloud liquid water content, rain intensity and sea ice parameters were documented by Basharinov et al. (1974). Many more passive microwave instruments have been flown, including early on the SEASAT and NIMBUS VII SMMR's mentioned in

the introduction. They have become the work-horses of satellite remote sensing of tropical cyclones, being based on well-established technology.

Advantages of microwave remote sensing from space are due to combination of several factors. Sensors can penetrate through clouds and low-intensity precipitation and estimate the water surface temperature and near-surface wind speed practically over the whole ocean. Multi-frequency measurements allow retrieval both of integrated parameters such as total atmospheric water vapor content, total cloud liquid water content and rain rate (satellite multi-frequency radiometers—sensors) and the vertical profiles of air temperature and humidity (sounders). The molecular oxygen absorption band (50–70 GHz) and a line (118.75 GHz) are well suited for temperature sounding due to O_2 being uniformly distributed within the atmosphere. These advantages are realized due to the state of the art of the current radiometer construction providing highly stable calibration during long-term operation in space that is necessary, in particular, for climate change studies and for providing a dependable data source when tropical cyclones threaten.

Passive microwave radiometers have a strong heritage of instruments: the Kosmos-243 four channel nadir-looking nonscanning microwave radiometer, the Meteor-18 and Meteor-28 two-polarization nonscanning microwave radiometers, the Indian Bhaskara I and II, two-channel microwave radiometers, the DMSP Special Sensor Microwave Imager (SSM/I), the Tropical Rainfall Measuring Mission (TRMM) Microwave Imager (TMI), the Advanced Earth Observing Satellite-II (ADEOS-II) Advanced Microwave Scanning Radiometer (AMSR), the Advanced Microwave Scanning Radiometer–Earth Observing (AMSR-E), the NOAA Advanced Microwave Scanning Units (AMSU-A and AMSU-B), the Special Sensor Microwave Imager/Sounder (SSM/I-S) and the multifrequency polarimetric microwave radiometer WindSat. These instruments measure horizontal (h) and/or vertical (v) polarized brightness temperatures $T_B^{V,H}$ over a range of frequencies, ν . WindSat also measures the cross-correlation of the vertical and horizontal polarizations. The cross-correlation terms represent the third and fourth parameters of the modified Stokes vector (e.g. Gaiser et al. 2004).

2.2.1.1 DMSP SSM/I

The SSM/I is a seven-channel, linearly polarized passive microwave radiometer aboard selected Defense Meteorological Satellite Program (DMSP) vehicles (Hollinger et al. 1990). The SSM/I is carried aboard the F8, F10, F11, F12, and F13 vehicles. Some of the channels on the F8 SSM/I are not operational. As an example orbital information for the F11 vehicle is as follows: maximum/minimum altitude: 878/841 km; inclination: 98.8°; period: 101.9 min and ascending equator crossing local time 18:11 (at launch). Other satellites except the F10 have similar orbits. The F10 did not achieve the desired orbit (more elliptical than desired), so orbital information given above is not applicable to the F10. Since 1987, the SSM/Is have proven to be stable, well-calibrated instruments whose data are useful for a variety of geophysical applications.

The SSM/I instrument consists of an offset parabolic reflector that is 61×66 cm fed by a seven-port horn antenna. The reflector and feed are mounted on a drum which contains the radiometers, digital data subsystem, mechanical scanning subsystem, and power subsystem. The drum assembly rotates about the axis of the drum. A small mirror and a hot reference absorber are mounted on the assembly. The instrument sweeps a cone around the satellite velocity vector so that the Earth incidence angle is always 53° . The SSM/I rotates continuously about an axis parallel to the local spacecraft vertical at 31.6 rpm. The SSM/I measures the upwelling brightness temperature over an angular section of 102.4° about the sub-satellite track. When looking in the forward direction of the spacecraft, the scan is directed from left to right with active scene measurements lying 51.2° about the forward direction. The resulting swath width is 1,400 km, which results in 24 h global coverage. The spacecraft sub-satellite point travels 12.5 km during the 1.9 s period. Data are recorded during the 102.4° of the cone when the antenna beam intercepts the Earth's surface (Hollinger et al. 1990).

Vertical and horizontal polarization measurements are taken for 19.4, 37.0 and 85.5 GHz channels and for the 22.2 GHz only at V-polarization. The channel IFOV varies with channel energy, position in the scan, along scan or along track direction and altitude of the satellite. The 85.5 GHz IFOV is the smallest with a 13×15 km, and the 19.4 GHz IFOV is the largest at 45×70 km. The 37.0 GHz IFOV is 30×38 km, and 22.2 GHz one is 40×60 km.

Because the 85 GHz IFOV is smaller, it is sampled twice as often, i.e., 128 times per scan. The sampling interval is 4.22 ms and equals the time for the beam to travel 12.5 km in the cross track direction. Radiometer data at the remaining frequencies are sampled every other scan with 64 uniformly spaced samples being taken and have an 8.44 ms interval. Scan A denotes scans in which all channels are sampled and Scan B denotes scans in which only 85.5 GHz data are taken. Thus, one data cycle consists of four 85.5 GHz scans and two scans of the 19.4, 22.2, and 37.0 GHz channels. The sensitivity of all channels is high and equal 0.4 K for 19.4 and 37.0 GHz and 0.8 K for the two other channels.

Remote Sensing System (RSS) has recently reprocessed the entire brightness temperature ($T_B^{V,H}$) data set using advanced calibration techniques, more rigorous quality control, and better geolocation. The new methods are applied to all the SSM/I channels, including 85 GHz. 21 years of SSM/I brightness temperatures are now available on hard disk arrays. The SSM/I time series consists of 6 satellites spanning the period from 1987 to the present, which in 2012 represents a total of 55 satellite years (http://www.ssmi.com/ssmi/ssmi_brightness_temperatures.html).

The data from the DMSP satellites are received and used at operational centers continuously for determination of position and intensity of TCs (<http://www.nrlmry.navy.mil/TC.html>), and for forecast of their evolution as well as for research (e.g. Ferraro 1997; Ferraro et al. 2005; Wentz and Spencer 1998; Mitnik et al. 2002; Chen et al. 2004; Liu et al. 2008a; Wimmers and Velden 2007).

2.2.1.2 SSMIS

The primary mission of the Special Sensor Microwave Imager/Sounder, SSMIS, instrument is to combine and extend the imaging and sounding capabilities of three previously separate DMSP microwave sensors: the SSM/T-1 temperature sounder, the SSM/T-2 moisture sounder, and the SSM/I. With improved temperature sounding capabilities, the SSMIS is capable of profiling the mesosphere, i.e. 10–0.03 mb. As such, the SSMIS is currently the only operational passive microwave sensor that can collect temperature measurements in the 40–80 km altitude range. In addition, SSMIS offers capabilities associated with radiometer channels having common fields of view, uniform polarizations, and fixed spatial resolutions across the active scene/scan sector, making it thus far the most complex and unique operational satellite passive microwave imager/sounder flown (Kunkee et al. 2008).

SSMIS is a 24-channel, passive microwave radiometer designed to obtain a variety of polarized atmospheric temperature, moisture, and land variables under most weather conditions. Channel frequencies range from 19 to 183 GHz and are obtained over a swath width of approximately 1,707 km. Detailed channel characteristics are provided in Table 2.1. As indicated in Table 2.1, the SSMIS channels correspond to four main categories of measurement parameters (Bell 2006): Lower Atmospheric Sounding (LAS), Upper Atmospheric Sounding (UAS), Environmental (ENV) and Imaging (IMA) data.

The SSMIS employs the same conical scan geometry and external calibration scheme as the heritage SSM/I instrument (Fig. 2.2). By employing the conical scan geometry of the SSM/I, the SSMIS maintains uniform spatial resolution, polarization purity, and common concentric Fields of View (FOV) for all channels across the swath (Kunkee et al. 2008).

Important information on SSMI and SSMIS can be found at web sites:

http://nsidc.org/data/docs/daac/ssmis_instrument/index.html

<http://www.ncdc.noaa.gov/oa/rsad/ssmi/gridded/index.php> (“Description of Global Gridded Products National Environmental Satellite, Data, and Information Service—NESDIS”) and

<http://www.ncdc.noaa.gov/oa/rsad/ssmi/swath/> (“SSMI and SSMIS Monitoring and Documentation”, NESDIS).

Application of SSMIS data to tropical cyclone study is considered by Hawkins et al. (2008).

2.2.1.3 AMSU-A and AMSU-B

The Advanced Microwave Sounding Unit (AMSU) is derived from the Microwave Sounding Unit (MSU) which began service in 1978 on TIROS-N and continued on the NOAA 6 through 14 satellites. AMSU flies on the NOAA 15, launched 13 May 1998; NOAA 16, launched 21 September 2000; and NOAA 17, launched 24 June 2002.

Table 2.1 Channel characteristics of the SSMIS instrument

Channel	Center frequency (GHz)	3-db width (MHz)	Polarization	NEAT (K) ^a	Sampling interval (km) ^b	Channel application
1	50.3	380	V	0.34	37.5	LAS
2	52.8	389	V	0.32	37.5	LAS
3	53.596	380	V	0.33	37.5	LAS
4	54.4	383	V	0.33	37.5	LAS
5	55.5	391	V	0.34	37.5	LAS
6	57.29	330	RCP ^c	0.41	37.5	LAS
7	59.4	239	RCP	0.40	37.5	LAS
8	150	1642(2) ^d	H	0.89	12.5	IMA
9	183.31 ± 6.6	1526(2)	H	0.97	12.5	IMA
10	183.31 ± 3	1019(2)	H	0.67	12.5	IMA
11	183.31 ± 1	513(2)	H	0.81	12.5	IMA
12	19.35	355	H	0.33	25	ENV
13	19.35	357	V	0.31	25	ENV
14	22.235	401	V	0.43	25	ENV
15	37	1,616	H	0.25	25	ENV
16	37	1,545	V	0.20	25	ENV
17	91.655	1418(2)	V	0.33	12.5	IMA
18	91.655	1411(2)	H	0.32	12.5	IMA
19	63.283248 ± 0.285271	1.35(2)	RCP	2.7	75	UAS
20	60.792668 ± 0.357892	1.35(2)	RCP	2.7	75	UAS
21	60.792668 ± 0.357892 ± 0.002	1.3(4)	RCP	1.9	75	UAS
22	60.792668 ± 0.357892 ± 0.0055	2.6(4)	RCP	1.3	75	UAS
23	60.792668 ± 0.357892 ± 0.016	7.35(4)	RCP	0.8	75	UAS
24	60.792668 ± 0.357892 ± 0.050	26.5(4)	RCP	0.9	37.5	LAS

^a NEAT for instrument temperature (0 °C) and calibration target (260 K) with integration times of 8.4 ms for channels 12–16; 12.6 ms for channels 1–7, 24; and 25.2 ms for channels 19–23 and 4.2 ms for channels 8–11, 17–18

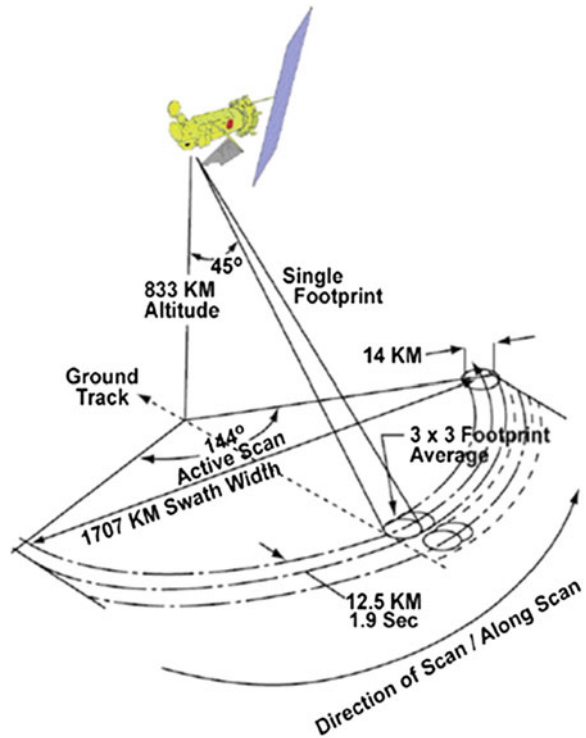
^b Along-scan direction sampling based on 833 km spacecraft altitude

^c RCP denotes right-hand circular polarization

^d Number of sub-bands is indicated by (n) next to individual 3-db width

AMSU has a finer vertical resolution with 15 channels for atmospheric temperature sounding. Using this new instrument, there are several techniques to estimate size, structure, intensity, wind speed in TCs, as well as to retrieve the global atmospheric temperature and humidity profiles from the Earth's surface to the upper stratosphere, at approximately 2-millibar pressure altitude. AMSUs are always situated on polar-orbiting satellites in sun-synchronous orbits and they cross the equator at the same local solar time at ascending and descending orbits. The AMSU has two sub-instruments, AMSU-A with 15 channels (23.8, 31.4, 89.0 GHz with V-polarization and 12 channels in oxygen absorption band between 50.3 and 57.6 GHz with H- or V-polarization) and AMSU-B with 5 channels (89.9, 150 GHz and three channels: 183.31 ± 1.00 , 183.31 ± 3.00 and 183.31 ± 7.00 GHz within a vapor absorption line, all with V-polarization). Swath width is equal to 1,650 km and IFOV at nadir for a nominal spacecraft altitude of 833 km is 48 km for AMSU-A which is twice that of MSU and it is 16 km for AMSU-B. The AMSU-A antenna provides a cross-track scan, scanning $\pm 48.3^\circ$ from nadir with a total of 30 Earth

Fig. 2.2 SSMIS Scan Geometry (Poe et al. 2001). Schematic of the sampling by the scanning microwave/imager sounder



fields-of view per scan line. The instrument completes one scan every 8 s. The AMSU-B antenna also provides a cross-track scan, scanning $\pm 48.95^\circ$ from nadir with a total of 90 Earth fields-of view per scan line. The instrument completes one scan every 2.66 s (Bennartz 2000; Kramer 2002).

AMSU applicability to retrieval of the oceanic and atmospheric parameters in the tropical zone and to TC analysis was shown by Knaff et al. (2000), Staelin and Chen (2000), Spencer and Braswell (2001), Demuth et al. (2004, 2006), and Bessho et al. (2006).

2.2.1.4 Suomi NPP, ATMS

The Suomi National Polar-orbiting Partnership or Suomi NPP, previously known as the National Polar-orbiting Operational Environmental Satellite System Preparatory Project (NPP) and NPP-Bridge is a NASA weather satellite which was launched on October 27, 2011 and was successfully inserted into its sun-synchronous low-Earth orbit. Three months after the satellite's launch it was named Suomi NPP after Verner E. Suomi http://en.wikipedia.org/wiki/Verner_E._Suomi, a meteorologist at the University of Wisconsin-Madison. The Suomi NPP is the first mission designed to collect critical data to improve weather

forecasts in the short-term and increase our understanding of long-term climate change. In the next decade, the Suomi NPP will be the principal U.S. operational, polar-orbiting, space-based observing system for weather forecasting and climate monitoring (Lee et al. 2010). The Advanced Technology Microwave Sounder (ATMS) sensor is designed for measurement of water vapor content at various altitudes of the atmosphere. The ATMS is a cross-track scanner with 22 channels that combine all the channels of the preceding AMSU-A1, AMSU-A2, and AMSU-B sensors into a single package with considerable savings in mass, power and volume (<http://npp.gsfc.nasa.gov/atms.html>). The 22 channels of the ATMS are divided into two groups: a low-frequency (23–57 GHz) group, and a high-frequency (88–183 GHz) group. The low-frequency channels, 1 through 15, are primarily for temperature soundings and the high-frequency channels, 16 through 22, are primarily for humidity soundings. ATMS will provide vertical temperature and moisture soundings across a swath width of 2,300 km. In comparison to heritage instruments, ATMS has an extended off nadir view angle, which will result in no gaps between successive orbits. ATMS will also be capable of retrieving surface precipitation rates, water path estimates for rain and snow, and peak vertical wind. Recent studies demonstrate that ATMS will perform better than AMSU for these retrieved precipitation parameters (Surussavadee and Staelin 2008).

2.2.1.5 ADEOS-II AMSR and Aqua AMSR-E

The AMSR was launched onboard the Advanced Earth Observing Satellite-II (ADEOS-II, Midori) on December 14, 2002 and the AMSR-E was launched onboard the Aqua satellite on May 4, 2002. On Aqua it is abbreviated as AMSR-Earth Observation System or AMSR-E; it is similar to SSM/I. AMSR-E takes dual-polarization observations at the 6 frequencies: 6.925, 10.65, 18.7, 23.8, 36.5 and 89.0 GHz. AMSR has two additional channels with V-polarization at the frequencies of 50.3 and 52.8 GHz. From an altitude of 705 km radiometers measure the upwelling Earth brightness temperatures with a resulting swath width of 1,445 km (AMSR-E) and 1,600 km (AMSR). The nadir angle is fixed at 47.4° which results in an Earth incidence angle of $55.0^\circ \pm 0.3^\circ$. During a scan period the sub-satellite point travels 10 km. The IFOV for each channel is different (Table 2.2), however, Earth observations are recorded at equal sample intervals of 10 km (5 km for the 89 GHz channels) along the scan. The sensitivity and other characteristics of the channels are given in Table 2.2 (Kawanashi et al. 2003). AMSR adopts the external calibration scheme which is similar to that of SSM/I. The Hot Load is maintained at a physical temperature of about 300 K, while the Cold Sky Mirror introduces the cosmic background radiation (approximately 2.7 K). Unfortunately, the AMSR mission ended in October 2003 and AMSR-E ceased observations on October 4, 2011.

Near real-time browse images of precipitation, water vapor, and track of the latest tropical cyclone observed by PR/VIRS (TRMM) and AMSR-E (Aqua) from developing to decaying stage was available till October 4, 2011 via “JAXA/EORC

Table 2.2 Characteristics of the AMSR and AMSR-E channels

Center frequency (GHz)	6.925	10.65	18.7	23.8	36.5	89.0	50.3/52.8
Bandwidth (MHz)	350	100	200	400	1000	3000	200/400
Polarization	V/H	V/H	V/H	V/H	V/H	V/H	V
Sensitivity (K, target)	0.3	0.6	0.6	0.6	0.6	1.1	1.8/1.3
IFOV (km × km)	71 × 41	46 × 26	25 × 15	23 × 14	14 × 8	6 × 4	12 × 6
Sampling rate (km × km)	10 × 10	10 × 10	10 × 10	10 × 10	10 × 10	5 × 5	10 × 10
Integration time (ms)	2.6	2.6	2.6	2.6	2.6	1.3	2.6

50.3/52.8 channels were at ADEOS II AMSR only

Real-Time Monitoring for Tropical Cyclones” (<http://sharaku.eorc.jaxa.jp/AMSR/relay/monitor.html>); Japan Aerospace Exploration Agency (JAXA)/Earth Observation Research Center. Thus, Real-time monitoring for tropical cyclones is now available. The coverage of AMSR-E has been expanded to the global coverage (June 1, 2011). JAXA EORC provides access to online archive of images, movies and data of tropical cyclones observed by TRMM/Aqua/Midori-II satellites (http://sharaku.eorc.jaxa.jp/TYPHOON_RT/index.html).

Applications of AMSR/AMSR-E data to tropical cyclones were considered in many journal and conference papers (e.g. Wilheit et al. 2003; Mitnik and Mitnik 2003, 2005b, 2010, 2011; Mitnik et al. 2005a, 2009; Shi and Wang 2007; Yan and Weng 2008; Greenwald 2009; Shibata 2006, 2009).

2.2.1.6 Coriolis/WindSat

WindSat is a satellite-based multifrequency polarimetric microwave radiometer developed by the Naval Research Laboratory for the U.S. Navy and the National Polar-orbiting Operational Environmental Satellite System (NPOESS) Integrated Program Office (IPO). It is designed to demonstrate the capability of polarimetric microwave radiometry to measure the ocean surface wind vector from space. WindSat is the primary payload on the Air Force Coriolis satellite, which was launched on 6 January 2003. It is in an 840-km circular Sun-synchronous orbit. Using a conically-scanned 1.83 m offset parabolic reflector with multiple feeds, WindSat covers a 1,025 km active swath. The 10.7, 18.7, and 37.0 GHz channels are fully polarimetric; that is, they derive all four Stokes parameters by measuring the six principal polarizations. The 6.8 GHz channel is dual polarimetric (vertical and horizontal) and provides sea surface temperature as a secondary product. The 23.8 GHz channel is also dual polarimetric because its purpose is to correct for atmospheric water vapor which is unpolarized. Gaiser et al. (2004) describe this passive microwave wind sensing instrument (Table 2.3) which allows to separate effects of wind speed and direction and therefore provides information of the wind vector.

Obtaining wind speed and direction from a passive sensor was proposed in order to save the great expense of launching scatterometers. Several retrieval algorithms were developed (e.g., Bettenhausen et al. 2006; Smith et al. 2006). The Coriolis has been in operation for several years and the data are used operationally,

Table 2.3 Characteristics of the WindSat channels

Frequency (GHz)	Polarization	Bandwidth (MHz)	Incidence angle (deg)	IFOV(km × km)
6.8	V, H	125	53.5	40 × 60
10.7	V, H, $\pm 45^\circ$, L, R	300	49.9	25 × 38
18.7	V, H $\pm 45^\circ$, L, R	750	55.3	16 × 27
23.8	V, H	500	53.0	12 × 20
37.0	V, H $\pm 45^\circ$, L, R	2,000	53.0	8 × 13

in particular, to retrieve wind vectors in tropical cyclone areas including rain conditions (Adams et al. 2006; Meissner and Wentz 2006, 2008; Knaff et al. 2011; Mims et al. 2010; Yueh et al. 2006). The experience does not indicate that the quality of WindSat wind retrievals is equivalent to scatterometer wind vectors.

2.2.1.7 Global Change Observation Mission-W1 AMSR2

The Advanced Microwave Scanning Radiometer-2 (AMSR2) will be launched as a single mission instrument onboard on the first satellite of the Water Series of Global Change Observation Mission (GCOM-W1). “Shizuku” (meaning a “drop” or a “dew”) was selected by the Japan Aerospace Exploration Agency (JAXA) as a GCOM-W1 nickname. GCOM is a series of JAXA Earth Observation Missions, successors to the ill-fated ADEOS-II satellite and to the Aqua Mission. GCOM is, together with the GPM Mission, Japan’s contribution to the Global Earth Observation System of Systems (GEOSS). The mission of GCOM-W1 is to observe the water cycle.

AMSR2 is multi-frequency, total-power microwave radiometer system with V- and H-polarization channels for all frequencies. Frequency channel set is identical to that of AMSR-E except 7.3 GHz channel for Radio Frequency Interference (RFI) mitigation (Table 2.4). It has a digitization at 12 bits and a dynamic range from 2.7 to 340 K. AMSR2 has two-point external calibration with the improved HTS (hot-load) and performs deep space calibration maneuvers to check consistency between main reflector and CSM (Imaoka et al. 2010; Oki et al. 2010). Scan angle is nominally 55° with an offset 2 m parabolic antenna, the world’s largest observation sensor aboard a satellite. The height of the rotating part is about 2.7 m and the weight is about 250 kg. The AMSR2 can keep rotating such a large and heavy antenna at a speed of one turn per 1.5 s for 24 h a day and more than 5 years without a minute of rest. It covers a swath width of 1,450 km. The AMSR2 can observe over 99 % of the Earth’s area in just 2 days. The GCOM-W1 AMSR2 data will continue valuable time series of quantitative observations of tropical cyclones which are collected since 2002 by Aqua AMSR-E (http://sharaku.eorc.jaxa.jp/TYPHOON_RT/index.html).

GCOM-W1 was successfully launched on May 18, 2012 with the H-2A rocket. JAXA will take about 45 days to insert the satellite into an orbit ahead of Aqua;

Table 2.4 GCOM-W1AMSR2 characteristics

Center frequency (GHz)	6.925/7.3	10.65	18.7	23.8	36.5	89.0
Polarization	V/H	V/H	V/H	V/H	V/H	V/H
Band width (MHz)	350	100	200	400	1,000	3,000
IFOV (km × km)	35 × 62	24 × 42	14 × 22	15 × 26	7 × 12	3 × 5
Sampling rate (km × km)	10 × 10	10 × 10	10 × 10	10 × 10	10 × 10	5 × 5

that is it will be in the so-called A-train (L’Ecuyer and Jiang 2010; Lee et al. 2012) in order to participate in an Earth observation mission called the “A-Train” in cooperation with satellites of other countries while performing the initial functional confirmation for about 3 months. NASA and its international partners operate several Earth observing satellites that closely follow one after another along the same orbital “track”. This coordinated group of satellites, constituting a significant subset of NASA’s current operating major satellite missions, is called the Afternoon Constellation, or the A-Train, for short. The Mean Local Time of the Ascending Node (MLTAN) of the GCOM-W1 orbit will be between (OCO-2—259.5 s) and (Aqua—79.5 s). It has a sun synchronous orbit (A-Train orbit). Altitude 699.6 km (on Equator), inclination 98.2°, local sun time: 13:30 ± 15 min. Five satellites currently fly in the A-Train: GCOM-W1, Aqua, CloudSat, CALIPSO, and Aura. Orbiting Carbon Observatory 2 (OCO-2) will join the configuration in 2013.

**2.2.2 *Passive and Active Microwave Systems
for Atmospheric Measurements***

2.2.2.1 CloudSat

The CloudSat Mission was jointly developed by the NASA/JPL and the Canadian Space Agency. CloudSat’s payload, the Cloud Profiling Radar (CPR), is the first spaceborne 94-GHz (W-band) radar and is contributing vertical cloud profiles (VCPs) over the globe (Stephens et al. 2002). CPR provides direct information on the vertical distribution of clouds and their optical and physical properties with unprecedented spatial and vertical resolution important for weather system analysis and forecasts (Stephens et al. 2002; Kim et al. 2011; Lee et al. 2012). Knowledge of the vertical cloud profiles, including parameters such as the cloud-top and cloud-bottom height and the cloud-layer thickness under various cloudiness conditions (e.g. semi-transparent/opaque clouds and multiple cloud layers), is necessary, in order to better understand complex cloud radiative forcing effects. The VCP affects atmospheric circulation by determining the vertical gradient of radiative heating/cooling and latent heating.

The Cloud Profiling Radar measures the returned backscattered energy by clouds as a function of height along the orbital track with a 240 m vertical range resolution

between the surface and 30 km along its flight path with footprint size of 1.4×1.7 km (Stephens et al. 2002, Tanelli et al. 2008). Unfortunately, it is only capable of quantitatively profiling lightly precipitating cloud systems (Mitrescu et al. 2010). For higher precipitation rates, complications arising from increased extinction and multiple scattering make quantitative precipitation analysis almost impossible. At rain rate exceeding 30 mm/h that is typical for typhoon eyewall and rain bands radar signals backscattered by the sea surface disappear due to very high two-way attenuation. Despite these limitations CloudSat profiles can show precipitation features such as melting layers (as bright bands, Matrosov 2010), deep convective towers, and multiple cloud layers. The capability to distinguish between convective and stratiform precipitating systems is also important for TC study.

2.2.2.2 Tropical Rainfall Measuring Mission

Most records of precipitation over the sea are based on indirect estimates by remote sensing using the cloud brightness or cloud top temperature as indicators of deep and raining systems (e.g. Adler et al. 2003). Direct measurements of precipitation over oceans are almost non-existent, and even attempts to put rain gauges on ships and buoys have had little success due to flow distortion by the ship's structure. Buoys also have issues with contamination by sea spray, so today satellite estimates of precipitation are typically calibrated against coastal radar estimates of precipitation, which in turn are calibrated against ground based rain-gauge networks (Adler et al. 2003). In spite of these difficulties we do now have precipitation estimates based on inferences from the temperature and patterns of cold cloud tops and from microwave radiometer measurements of the cloud water particles and scattering by large ice particles. (These are airborne precipitation particles, which may or may not coincide with precipitation impacting on the sea surface). A method for estimating the ground precipitation combining various methods called CMORPH (which stands for CPC Morphing technique, where CPC is Climate Prediction Center), has been developed for routine use (Joyce et al. 2004). It is flexible, because it can combine various measurements and their algorithms by "morphing" them together.

A dramatic step forward in rain measurements over the oceans from space was provided by the Tropical Rainfall Measuring Mission, TRMM (Simpson et al. 1988; Kummerow et al. 1998; Kummerow et al. 2000) which carried a narrow-swath rain radar (215 km) and the TRMM Microwave Radiometer, TMI, with a 760 km swath width. It was launched in November 1997 and provided data for a decade. The satellite had a low-earth (402 km height), non-polar orbit that allowed it to sample low latitude regions at different times in the diurnal cycle during a month's time. It outlived its scheduled life-time and has continued operations at a lower altitude (350 km) with somewhat reduced functions. It has been used at operational centers when available, but was not intended to be an operational weather satellite, being that its revisit times for the same location takes a whole month. The goal was to obtain climatology of tropical and subtropical precipitation. One of its major contributions was its calibration of the microwave

radiometer algorithms and the additional insight into storm structure that its vertical resolution provided. See further [Sect. 2.3.5](#).

The TRMM Microwave imager: The TMI is a nine-channel passive microwave radiometer based upon the DMSP SSM/I. The key differences are the addition of 10.7-GHz channels with V- and H-polarizations and a frequency change of the water vapor channel from 22.235 to 21.3 GHz. This change off the center of the water vapor line was made in order to avoid saturation in the tropical orbit of TRMM. Additionally, this provides improving the accuracy of total water vapor retrieval (Mitnik and Mitnik 2006). Table 2.2 presents the performance characteristics of the nine TMI channels (Kummerow et al. 1998). The increased spatial resolution evident in Table 2.2 is due to the lower orbit of the TRMM satellite with respect to the DMSP rather than sensor differences (Table 2.5).

Combination of passive and active microwave sensing has proved its high efficiency for precipitation study. This approach will be advanced at the Global Precipitation Measurements (GPM) project. GPM is designed to make more accurate and frequent observation of tropical rainfall by expanding its observing areas to higher latitudes. GPM is composed of one core satellite and approximately eight constellation satellites. The core satellite carries a Dual-frequency Precipitation Radar (DPR) and a microwave radiometer will be used to measure precipitation structure and to provide a calibration standard for the constellation satellites with microwave radiometers. The core satellite is scheduled for launch in early 2014 and the low-inclination satellites for launch in November 2014 (<http://science.nasa.gov/missions/gpm/>).

2.2.3 Variables Retrieved by Microwave Radiometers, Sounders, CloudSat and TRMM

2.2.3.1 Ocean Surface

Several geophysical variables can be retrieved from the microwave sensors. Sea surface temperature was a very desirable quantity, because infrared signals emitted from the sea surface, already well established technology, were cut-off by clouds.

Table 2.5 TMI characteristics

Center frequencies (GHz)	10.65	19.35	21. 3	37.0	85.5
Bandwidth (MHz)	100	500	200	2000	3000
Polarization	V/H	V/H	V	V/H	V/H
Sensitivity (K)	0.63/0.54	0.50/0.47	0.71	0.36/0.31	0.52/0.93
IFOV (km × km)	63 × 37	30 × 18	23 × 18	16 × 9	7 × 5
Sampling interval (km × km)	13.9 × 9.1				13.9 × 4.6

The incidence angle of the antenna beam is 52.88 at the earth’s surface and a swath width is 758.5 km. TMI swath covers precipitation radar (PR) swath that is equal to 215 km as shown in Fig. 3 (Kummerow et al. 1998)

This has resulted in biased observations because they could only be obtained outside storms. Microwaves at low frequencies (of the order of 5 and 6 GHz) penetrate with little absorption through clouds (less so through rain) and recent sensors allow to retrieve SST under cloud conditions and estimate ocean surface thermal variability caused by diurnal heating or wind action in the wake of hurricanes and typhoons (Wentz et al. 2000; Gentemann and Minnett 2008; Gentemann et al. 2008, 2010a, b; Reynolds et al. 2007, 2010; Shibata 2009).

Sea surface wind response by passive microwave radiometers was deemed to be caused by the increased emissivity of the sea surface when white caps form and there is foam on the sea surface. This indicates that the state of the sea, which is not always simply related to the mean wind speed, contributes some uncertainty in the inversion algorithms. However, on the open ocean much of the variability is averaged out by the relatively large footprints required for the lower frequencies used for wind speed (6.9–37 GHz) on above described radiometers SSM/I, TMI, SeaWinds, AMSU, AMSR-E (Sasaki et al. 1987; Krasnopolsky et al. 2000; Azis et al. 2005; Bessho et al. 2006; Shibata 2006; Boukabara and Weng 2008; Mitnik and Mitnik 2010, 2011). In fact, the physics of the measurement is not used in the calibration for wind speed, but conversion to geophysical information resorts to empirical fits between satellite microwave measurements and surface observations. The sophisticated use of the Stokes parameters in WindSat provides information of speed and direction from this instrument, but it has greater limitations compared to the scatterometers, due to atmospheric interference.

2.2.3.2 Atmospheric Integrated Water Vapor, Cloud Liquid Water Content and Precipitation

Satellite passive microwave data are unique in being able to provide large-scale maps of integrated water vapor, V , and integrated cloud liquid water, Q , independently of time of a day and under cloudy conditions. V and Q over the oceans have been successfully retrieved from satellite microwave measurements carried out by multichannel microwave radiometers on board “Kosmos-243”, Nimbus 7, DMSP series satellites, TRMM, Aqua, ADEOS-II, WindSat, NOAA, TOPEX, Jason and several other satellites. Nevertheless despite comparatively long history of satellite passive microwave observations and their advantages, the interpretation of data from microwave sensors always had large errors under significantly changing environmental conditions (Wentz 1997) and has always been limited in ocean areas with heavy rain, which are typical for tropical cyclones and for the Intertropical Convergence Zone. To estimate water vapor and cloud liquid water in various marine weather systems and, especially, climatic trends from satellite passive microwave data, there is a strong need in having precise retrieval algorithms tuned. Many algorithms exist for retrieval of the integrated water vapor V and integrated cloud liquid water from satellite passive microwave measurements.

Some of the algorithms are based on purely statistical techniques, the starting point of which is a database containing both brightness temperatures $T_B^{V,H}(v_i)$ and

the corresponding environmental conditions for global or for the specific regions such as the tropics. Such a method can easily be used for V , by collocating ship and small island radiosondes with satellite overpasses. The brightness temperatures can also be computed using a state of the art model of microwave radiative transfer in the atmosphere–ocean system. Due to the lack of any routine measurement of cloud liquid water, a reasonable approach is construction of cloud liquid water content profiles using the radiosonde profiles of air relative humidity and temperature, information on the amount and forms of clouds and generalized data on their liquid water content (Mitnik and Mitnik 2003). The inversion is then performed using a statistical method, with or without a priori choice of channels or functions of the channels. As the V retrieval is close to linear, a simple multi-linear regression on $T_B^{V,H}(v_i)$ has often been used.

The most well-known purely statistical algorithms for SSM/I are those of Alishouse et al. (1990a, b) for water vapor, which is a linear combination of T_B^V at 19, 22 and 37 GHz channels, with addition of a quadratic term in $T_B^V(22)$ to better account for the non-linearity, and for Q , as linear function of brightness temperatures $T_B^V(19)$, $T_B^H(19)$, $T_B^V(37)$ and $T_B^H(85)$.

Alishouse et al. (1990a) algorithm is used up to now to retrieve total water vapor content from SSM/I and AMSR-A brightness temperatures and get animations of global and regional V -fields (Wimmers and Velden 2007) showing, in particular, evolution of tropical cyclones and their interaction with other atmospheric pressure systems and the ocean (<http://tropic.ssec.wisc.edu/real-time/mimic-tpw/global/main.html>).

The other ones are physically-based, resting on the Radiative Transfer Equation (RTE) simulations (Mitnik 1969; Basharinov et al. 1974; Greenwald et al. 1993; Wentz 1992, 1997; Petty and Katsaros 1992; Liu and Curry 1993; Grody et al. 2001; Ferraro et al. 2005; Horváth and Davies 2007; Mitnik and Mitnik 2003, 2006, 2010; Meissner and Wentz 2006; O'Dell et al. 2008; Yan and Weng 2008; Weng et al. 1997, 2003, 2007). The established advantage of physically-based algorithms is their well developed theoretical basis and physical background of each step.

Neural Networks (NNs)-based algorithms can also be both statistically and physically-grounded. Their general point is that they don't require a *priori* knowledge of the transfer function, which can be of any non-linear character. This method has been used successfully in a large variety of remote sensing applications, including our specific case of V - and Q -parameter retrievals (Jung et al. 1998; Krasnopolsky et al. 2000; Mallet et al. 2002; Moreau et al. 2002; Bobylev et al. 2010).

Absorption spectrum by small cloud droplets is determined by the spectrum of the dielectric permittivity of fresh water $\varepsilon(v)$ that, in turn, depends on the temperature of cloud droplets t_{cl} (Mitnik 1978; Mitnik and Mitnik 2010; Mätzler et al. 2010). Uncertainties in ε values, especially for the temperatures below -20°C increase the errors of both T_B s simulation and the satellite-derived Q values. There is no information on vertical distribution of liquid water in thin clouds in the microwave observations (Ebell et al. 2010).

The uncertainty in the water vapor emission model is the dominant error source for the satellite-derived V values. An improved model of microwave absorption in the atmosphere will result in better retrievals of V , Q , W and sea surface emissivity, all of which are important applications of microwave remote sensing (Turner et al. 2009; Liu et al. 2011).

The emissivity of the calm sea surface is determined by the spectrum of the dielectric permittivity of saline water that, in turn, depends on its temperature and salinity (Liu et al. 2011). Experimental and theoretical research on the emissivity of the rough sea surface under variable environmental conditions continues. There remain discrepancies in published data and theories that emphasize the difficulties in performing accurate experiments and arrive at their theoretical description (Webster et al. 1976a; Sasaki et al. 1987; Aziz et al. 2005; Shibata 2004, 2006; Uhlhorn et al. 2007; Boukabara and Weng 2008; El-Nimri et al. 2010; Liu et al. 2011). Problems increase at high winds and intense wave breaking that is typical for the tropical cyclone areas (Shibata 2006; Uhlhorn et al. 2007; Yan and Weng 2008; Mims et al. 2010).

Typical values of total water vapor content in tropical cyclone areas change from 40 to 50 kg/m² at the periphery of a vortex and in a band of dry air frequently observed in TC circulation system to high values of 60–70 kg/m² in the central area and in spiral rain bands. The values of total cloud liquid water content can reach 2 kg/m² and more in the eye wall and in rain bands. Clouds with high Q -values are surrounded by clouds with the lower Q values that, in turn, are imbedded in the moist air mass. Typically the size of the area with the increased V -values is significantly larger than the area with $Q > 0.5$ kg/m². Retrieval of V and Q values at the areas of high atmospheric attenuation caused by water vapor, clouds and precipitation over the sea surface disturbed by storm winds is a complicated task. Nonetheless, great progress has been made as illustrated in Sect. 2.4.

2.2.4 Scatterometry

2.2.4.1 Satellite Instruments 1978–Present

Scatterometer instruments were developed to infer the surface wind vectors over the oceans from space. The principle of their operation was famously illustrated by the scatterometer on the SEASAT satellite in 1978 (e.g. Jones et al. 1982, and review by Katsaros and Brown 1991), but had earlier been proven by circle flights with a prototype radar. The relative position between radar look direction and the wind direction showed clear effects on the radar “backscatter”, a diffuse radar return, different from reflection. The SEASAT satellite carried the well established visible and infrared sensors, as well as several experimental instruments including a Ku-band scatterometer, i.e. a radar system consisting of 3 “stick” antennae, whose returns depend on the roughness of the sea and from which wind vectors (wind speed and direction) can be inferred. (Full discussion of the physics and

techniques as well as other issues in this section can be obtained from the excellent text by Robinson (2004). The SEASAT Ku-band scatterometer data allowed scientists to learn how to interpret radar returns from 3 stick antennae, as they consecutively viewed the same area on the sea surface under the advancing satellite. The algorithm should return wind speed and direction by inverting an empirical model relating measured scatterometer backscatter coefficients (in a matrix obtained by the 3 forward looking antenna and the 3 backward looking antenna observing the same pixel on the sea surface) and the comparison data on surface wind speed and direction. The geophysical model-function, GFM, is calibrated by use of in situ and/or output from atmospheric numerical models collocated in space and time with scatterometer measurements (e.g. Bentamy et al. 1999; Stoffelen 1999; Wentz et al. 2001). Since 1991 there have been several scatterometers in space, two from the European Space Agency, ESA, on the European Remote Sensing satellites 1 and 2, ERS 1/2, launched in 1991 and 1995, respectively. This ESA scatterometer, the Advanced Microwave Instrument (AMI) “sees” well through clouds since it is based on C-band radar technology, but such scatterometers are relatively insensitive to the small ocean waves at low wind speeds, while the Ku-band instruments are more adversely impacted by clouds and precipitation, but respond better to the small waves or roughness elements at low wind speeds. A Japanese–U.S. collaboration lead to the launch of Ku-band scatterometers, NSCAT (NASA scatterometer) on the Advanced Earth Observing Satellite (ADEOS) in 1996. Unfortunately, ADEOS I had an early demise, which lead to the fast launch in 1999 of QuikSCAT, a NASA satellite carrying the SeaWinds, a scanning scatterometer. This scatterometer was a copy of the instrument designed for ADEOS II, which was launched in 2002, Fig. 2.3. The SeaWinds on QuikSCAT was very successful (e.g. Ebuchi et al. 2002; Katsaros et al. 2001).

It collected data for a full 10 years allowing many new analysis techniques and algorithms to be tested. For example, Long (2004) achieved higher spatial resolution by sophisticated processing of the original data. When ADEOS II was flying its scatterometer, there was a period of a tandem sampling by two identical scatterometers, until ADEOS II also met an early demise (Liu et al. 2008b). The SeaWinds scatterometer has a continuous 1,800 km wide swath, including the nadir region, which has proven very important. One such instrument views the global ocean once every 12 h at 50° latitude, but less frequently in the tropics. The sampling with several scatterometers is highly desirable due to the rapidly changing wind field at any one location.

Since October 2007, the new Advanced Scatterometer, ASCAT, onboard MetOp-A, launched by EUMETSAT, is collecting data for an operational agency. EUMETSAT is the European organization for meteorological satellites for weather, climate and environmental applications. It provides valuable surface wind information with high spatial and temporal resolution over the global ocean using two C-band beams, each side of nadir. MetOp, Europe’s newest weather satellite, was successfully launched on 17 September 2012. Metop-B will first follow and then replace its identical twin, Metop-A, in a polar, sun-synchronous orbit.

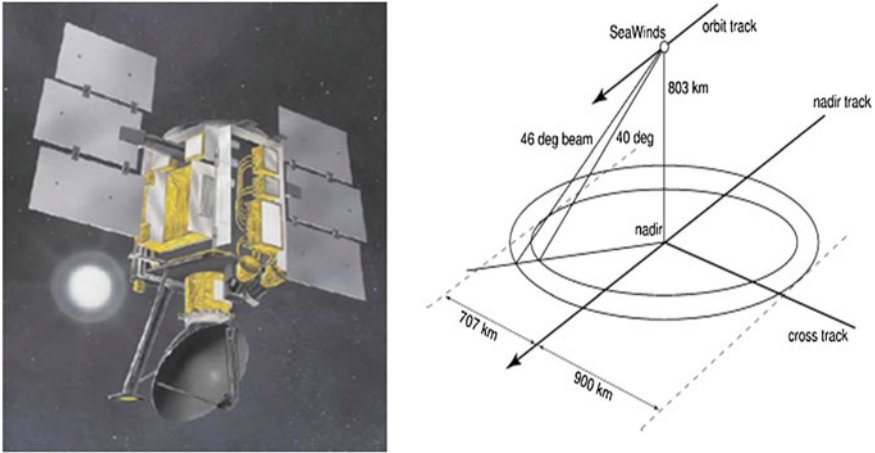


Fig. 2.3 SeaWinds on QuikSCAT satellite illustrating the sampling cone. *Left* The SeaWinds instrument on board QuikSCAT. The rotating disk antenna is 1 m in diameter (courtesy NASA/JPL). *Right* A schematic of the measurement geometry of the SeaWinds instrument on board QuikSCAT (from Freilich and Dunbar 2000). As indicated in the figure the far swath extends from 700 to 900 km on either side. The nadir swath is 499 km wide, centered on nadir

2.2.4.2 Wind Stress Versus Wind Speed

Interpretation and use of scatterometers data requires use of an atmospheric boundary layer model and understanding of the physics of the measurement. It was clear from the beginning that the backscatter signal being dependent on the sea surface roughness dominated by small waves, gravity and capillary waves, in a wavelength band that resonates with the radar's wavelength requires a direct relationship of these waves to the quantity of interest, which could be mean wind speed at a certain height or the wind stress at the sea surface. The short waves are generated by the local wind forcing of the ocean and are therefore related to the surface stress exerted by the atmosphere. A complexity arises due to some of the atmospheric stress being carried by the form drag due to larger waves, especially at high wind speeds. The conversion of the radar backscatter to a wind stress or wind speed is therefore rather complex and one "model function" may not be universally applicable. However, experience has shown that the current formulations for the different scatterometer systems perform quite well. They are strictly empirical fits and therefore depend on the quality of the "comparison data" from the sea surface.

Once we accept that the scatterometer measures wind stress, we then often need to convert it to a wind speed for many practical purposes, not least of which is for calibrating with the comparison data, which often is simply mean wind speed (and direction). That conversion involves use of a boundary layer model, since the wind speed at any one height also depends on the atmospheric stratification as defined in Monin–Obukhov theory (e.g. Businger et al. 1971). The equivalent Neutral wind

speed is that speed in neutral atmospheric stratification that would give the same stress as the scatterometer measured. The convention is to translate the comparison data to the value of the “equivalent neutral wind” at 10 m height before the inversion of the backscatter signals take place (e.g. Liu and Tang 1996). Thus, it is this Equivalent Neutral Wind speed and direction that is the output of the model function. It often involves up to 3 “aliases”, since the uncertainty in the signals, the comparison data and in the model function itself sometimes returns more than one plausible solution. Methods to eliminate the false aliases have been described (e.g. Woiceshyn et al. 1986). Currently the TOGA Coare3.0 boundary layer algorithm (Fairall et al. 2003; Bentamy et al. 2003) is used to convert the comparison data to 10 m neutral wind speed, when algorithms are tested and verified. However, sometimes the atmospheric stratification is not available, which makes the intercomparison inexact (W. T. Liu, personal communication, 2012).

The typical credentials for scatterometers have included wind speed accuracy of 2 m s^{-1} and wind direction within 20° (e.g. Jones et al. 1982; Ebuchi et al 2002). More complex concerns stem from the inherent limitation of the physics in that the wind speed measured is really the difference between the wind stress on the surface and the current vector in the sea (Liu et al. 2008a, b). The effects of the stratification in patterns of strong sea surface temperature gradients can also show up as variability in the surface wind as interpreted from the scatterometers (equivalent neutral 10 m wind, which can be directly converted to friction velocity). This variability can result from the atmospheric stress being transferred differently to the surface in stable and unstable sections of the field of view. For many application the 10 m neutral wind or the wind stress is the quantity of interest, but if the actual wind, say at 10 m height or any other height is needed, additional information on the atmospheric temperature gradient (and to a lesser extent the humidity gradient) must be furnished. The articles by Liu et al. (2008b) also discuss the role of inadequate sampling by just one scatterometer for many purposes and the opportunity to enhance the sampling by coordination between many satellite wind sensing systems.

2.2.5 *Synthetic Aperture Radars, SARs*

The active microwave sensors such as altimeters, scatterometers and Synthetic Aperture Radars (SARs) (Campbell 2002; CCRS 2009; Jackson and Apel 2004) are radars operating in the microwave region (1–30 GHz in frequency, 1–30 cm in wavelength) at different polarizations and incidence angles. Over the sea, the radar return depends, on the degree of development of the sea surface roughness (Valenzuela 1978). The roughness is composed of centimeter-decimeter water waves produced by the wind. Since the wind field has its own spatial pattern, which depends on its strength, on the thermodynamic characteristics at the air-sea interface and on the interaction between the wind flow and the orography near coastlines or islands, it generates certain spatial features. The radar backscatter

reacts to the sea surface roughness. Therefore, the study of the characteristics of the radar backscatter provides information on the characteristics of the wind and of the Marine Atmospheric Boundary Layer (MABL, see e.g. Katsaros et al. 2000). In this layer, important exchanges of sensible and latent heat, CO_2 and momentum take place over a large spectrum of temporal frequencies and spatial scales. It is the wind stress that drives the surface waves and the ocean drift currents (e.g. Bentamy et al. 2003; Zecchetto 2010; Baklanov et al. 2011; Liu and Xie 2008).

At present, there are several satellites equipped with Synthetic Aperture Radar (SAR) instruments: the European ENVISAT launched in March 2002 (ESA 2002), the German TerraSAR-X launched by Deutsche Luft und Raumfahrt in June 2007 (Buckreuss et al. 2003), the Italian Constellation of Small Satellites for Mediterranean basin Observations (COSMOSkyMed or CSK), developed by the Agenzia Spaziale Italiana (ASI) (since June 2007) (Coletta et al. 2007), the Canadian commercial satellite RADARSAT-1 (launched in November 1995) and RADARSAT-2 (launched in December 2007) (Morena et al. 2004), the Indian RISAT launched in April 2012. Below only the Envisat Advanced SAR (<http://envisat.esa.int>) and RADARSAT-1 and-2 SAR instruments (Hurley 2010) operating at C-band will be considered, since they have wide swath mode with swath width of 400 and 500 km and SAR image can cover a significant part of a tropical cyclone. Spatial resolution is approximately 150 by 150 m for Envisat ASAR and 100×100 m for RADARSAT-1 and -2 SARs (Fig. 2.4). In the Wide Swath Mode, the ScanSAR technique is used, providing images of a wider strip (405 km)

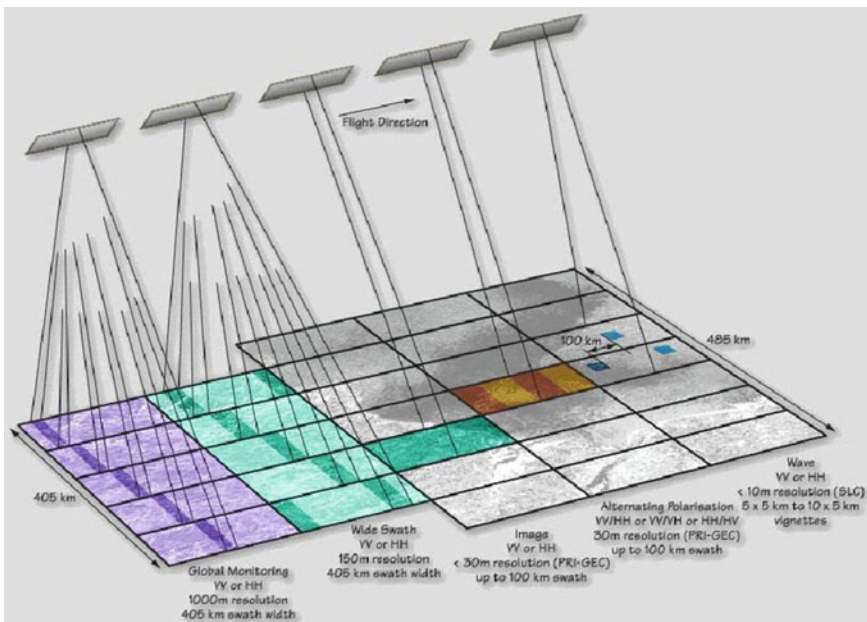


Fig. 2.4 Envisat ASAR operating modes

with medium-resolution (150 m) in HH or VV polarisation. The total swath consists of five subswaths and the ASAR transmits bursts of pulses to each of the subswaths in turn in such a way that a continuous along-track image is built up for each subswath.

The increased availability of satellite SAR images offers to scientists many opportunities to investigate the structure of the Marine Atmospheric Boundary layer, MABL, in tropical cyclones. Scientific literature about SAR images over the ocean has shown a variety of geophysical phenomena detectable by SAR (e.g. Jackson and Apel 2004), including the multi-scale structure in the atmospheric turbulence under high winds and the structure of the convective turbulence under low wind.

Satellite based Synthetic Aperture Radar (SAR) can operate day and night and in all weather condition. Radar signals penetrate clouds and precipitation that presents important advantage for tropical cyclone study compared to visible and infrared sensor such as AVHRR and MODIS. Furthermore, radars are truly sensing the surface and therefore observe the impact of the atmosphere on the ocean surface.

The high-resolution of SAR wind retrievals make these data suitable for understanding tropical cyclone wind and precipitation structure. Examples of high-resolution Envisat SAR images show the details which SARs can measure in examples from Northwest Pacific typhoons Aere and Songda in 2004 (Mitnik et al. 2005a), Talim and Matsa in 2006, Sinlaku in 2008 (Dagestad et al. 2010), Parma in 2009, Megi in 2010 (reported on in this chapter, Sect. 2.4) as well as Atlantic hurricanes such as Katrina in 2005 (Repucci et al. 2010).

2.2.6 Altimeters

Altimeters measure the height of the satellite above the sea surface, as the name implies. They obtain a narrow swath of 7 km width in the nadir track of the polar orbiting satellites that carry them. Satellite altimeters are designed to deliver relatively long revisit (10 days and more) and global views of sea surface height. The concept is well established since early missions GEOS-3 and SEASAT that date back to the 1970s. The launch of the TOPEX/Poseidon in 1992 provided the greatest impetus for satellite altimetry research in the 20th century. Its launch was followed by the Jason-1 (2001) and Jason-2 (2008). The European space Agency, ESA, satellites were launched in 1991, 1995, 2002, 2010 (ERS-1, ERS-2, ENVISAT, Cryosat-2) and the US Navy launched a series of Geosat satellites (1985 and 1998). Additional missions are planned in order to provide continuous coverage, e.g., AltiKa, Sentinel-3, HY-2, including new experimental concepts such as SWOT (Fu et al. 2009), which uses multiple frequencies and sampling by a scanning antenna. To date satellite altimetry has focused in the open ocean (Fu and Cazenave 2001), but interest in coastal observation is leading to new research (e.g. Vignudelli et al. 2011). An uninterrupted flow of altimeter data has been accumulating, contributing to the ability to address scientific and societal challenges related to the ocean. However, in some cases the various missions were designed

without continuity in mind, with different observing strategies usually driven by their particular objectives of accuracy, spatial resolution and temporal revisit requirements. For example, the T/P and Jason series main objective was to generate the best estimates of sea level over time to serve climate monitoring, but these data can be also used to better understand the ocean circulation. As a result, data from the various satellite altimeters were processed independently. Nevertheless, the missions have common foundations concerning retrievals, orbits, geophysical corrections, data calibration and exploitation. Very useful and unique information on tropical cyclones derived by altimeters includes accurate wind speed and sea state data along their tracks the width of 5–10-km (Quilfen et al. 2010; 2011).

2.2.7 Airborne Radiometers for Surface Wind

Stepped Frequency Microwave Radiometer (SFMR) and Hurricane Imaging Radiometer (HIRAD), history and instrument descriptions. Estimating hurricane surface wind distributions and maxima is an operational requirement of the Tropical Prediction Center/National Hurricane Center (TPC/NHC), and emergency management decisions rely on coastal watches and warnings issued by NHC based partly on observed winds. Surface wind speed estimates by NHC are determined largely from extrapolated aircraft flight-level wind data. In 1997, Global Positioning System (GPS) dropwindsondes (Hock and Franklin 1999) first demonstrated the ability to provide in situ measurements of hurricane surface wind velocities, most importantly in the inner core, and recent work utilizing these measurements has improved the accuracy of extrapolations (Franklin et al. 2003).

Since 1984, the Stepped Frequency Microwave Radiometer (SFMR) has flown on at least one of two NOAA WP-3D research aircraft to estimate hurricane surface wind speeds (Uhlhorn and Black 2003). Beginning in 2004, a redesigned SFMR was flown on one WP-3D aircraft for operational surface wind speed measurements. After procedural testing during 2004, both WP-3Ds had operational SFMRs installed in 2005. The unusually active 2005 Atlantic hurricane season provided ample opportunity to evaluate the SFMR performance over the entire range of expected surface wind speeds (10–70 m/s). In particular, extreme wind speed (>60 m/s) measurements were obtained from flights into Saffir–Simpson (SS) category 5 Hurricanes Katrina and Rita.

Since hurricane reconnaissance began in 1947, numerous methods have been employed to estimate the distribution of surface winds in hurricanes. Sea state catalogs have provided a guide to determination of the wind speed (Black and Adams 1983). For many years surface winds have been estimated by flight-level measurements using various extrapolation algorithms (Miller 1958; Powell 1980; Powell et al. 1996). Maximum sustained winds have been estimated using pressure–wind relationships summarized by Harper (2002) and most recently described by Knaff and Zehr (2007). In studies prior to 1980, Basharinov et al. (1974), Nordberg et al. (1969), Ross and Cardone (1974) and Wilheit (1979) showed that passive microwave emissions from the sea surface are also strongly correlated with wind speed.

The concept for the first experimental SFMR was proposed by C. T. Swift at the University of Massachusetts Microwave Remote Sensing Laboratory (C. T. Swift 1976, personal communication) and built by the National Aeronautics and Space Administration's (NASA) Langley Research Center in 1978 (Harrington 1980). The SFMR design involved a single nadir-viewing antenna and receiver capable of making measurements of radio emission from the sea surface at four selectable frequencies between 4.5 and 7.2 GHz. The "stepping" procedure allowed for estimating the surface wind speed in hurricanes by correcting for rain-induced effects in the measurements, and therefore enabling recovery of the rain rate. The first measurements by the original SFMR were made from the National Oceanic and Atmospheric Administration (NOAA) WC-130 aircraft in Hurricane Allen in 1980 and reported by Jones et al. (1982), as well as Black and Swift (1984), Delnora et al. (1985), and Swift and Goodberlet 1992). By making assumptions about the vertical structure of the atmosphere together with SST measurements by a downward-looking airborne infrared radiometer, reasonable estimates of the ocean surface brightness temperature (TB) were made at 4.5, 5.0, 5.6, and 6.6 GHz. Wind speeds were then calculated assuming a linear increase in wind speed with TB, independent of frequency. Agreement between surface (20 m) winds extrapolated from the 1,500-m flight level and the SFMR estimates for independent flight legs were within 6–10 %. Despite the success in Allen, this instrument was never again flown into a hurricane.

The SFMR measures nadir brightness temperature (TB) at six C-band frequencies, and a retrieval algorithm uses a Geophysical Model Function (GMF) relating surface emissivity and wind speed to produce surface wind speed estimates along the flight track. Early emissivity/wind speed models used in microwave radiometry applications have been developed for winds <25 m/s (Goodberlet et al. 1989; Wentz et al. 1986; Wentz 1983; Webster et al. 1976a), or either relied upon or were validated against aircraft flight-level high wind data extrapolated to the sea surface (Uhlhorn and Black 2003; Tanner et al. 1987; Black and Swift 1984; Swift et al. 1984; Jones et al. 1981). These early methods resulted in considerable uncertainty about the retrieved hurricane surface wind speed, especially under extreme conditions.

A second SFMR was designed and built in 1982 under the supervision of Swift (Swift et al. 1986). The number of frequencies was expanded to six between 4.6 and 7.2 GHz, and the instrument integration time was reduced to less than 1 s, resulting in improved spatial resolution. A new retrieval algorithm was also implemented and described in Tanner et al. (1987). This instrument was flown on board the NOAA WP-3D in 1984 and during 12 flights during the 1985 hurricane season. The SFMR was further modified in 1986 and initially used for studies of sea ice structure (St. Germain et al. 1993). Using data obtained in Hurricanes Earl (1985), Gilbert (1988), and Hugo (1989), the empirical emissivity–wind speed relationships were refined to include winds over 60 m/s. With support from the Office of the Federal Coordinator for Meteorology (OFCM) the existing horn antenna was replaced with a dipole array antenna in 1993. The new antenna with a new set of six frequencies was flown in Hurricane Olivia (1994) and retrieved high

quality wind estimates. Further funds were provided by OFCM for an upgrade of the SFMR's receiver, which allowed for increased calibration stability. The reconfigured SFMR (Goodberlet and Swift 1996) was first flown in Hurricane Jerry in 1995. Minor modifications were made to reduce background noise levels after the 1995 season.

The Stepped Frequency Microwave Radiometer represents a potentially significant advancement in the remote measurement of hurricane near-surface wind speeds, most notably at speeds >50 m/s. This improvement is due to both refined remote sensing technologies, and more accurate ground-truth data in the form of GPS dropwind-sonde wind speed measurements. The SFMR yields wind speed measurements that are overall within ± 4 m/s rms of the dropwind-sonde-estimated surface wind. Figure 2.5 illustrates the cross-track scanning ability of the new Hurricane Imaging RADiometer (HIRAD) based on a WP-3D installation compared to the nadir-viewing SFMR. The figure also shows the sampling of the

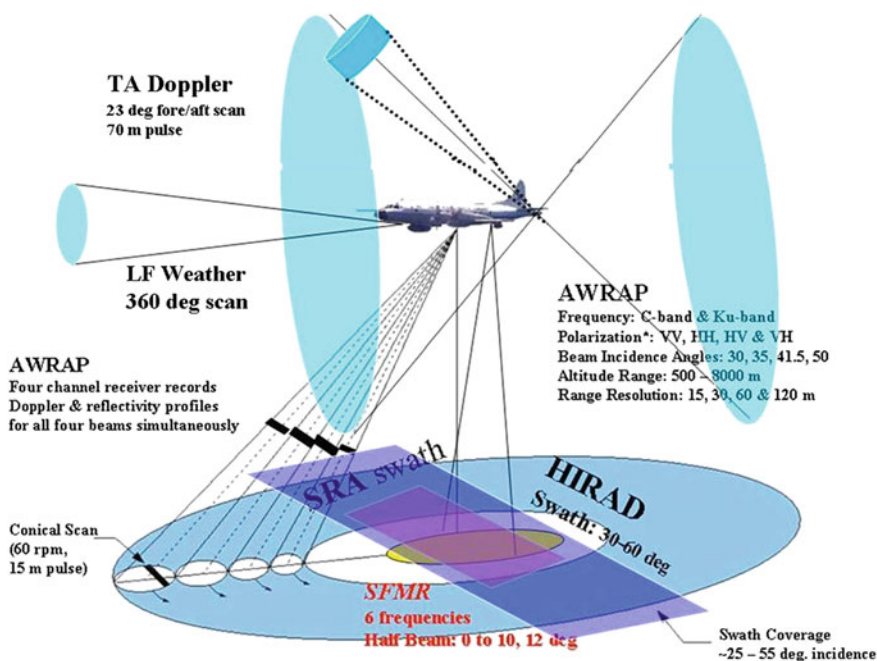


Fig. 2.5 Remote sensing instruments on the NOAA WP-3D aircraft. These include the 360° scanning lower fuselage (LF) for vertically integrated radar reflectivity mapping; the Tail (TA) Doppler radar for 3-D wind and reflectivity mapping (0.5–12 km altitude); stepped frequency microwave radiometer (SFMR—yellow oval swath) for surface wind and integrated rain rate; wideswath scanning radar altimeter (WSRA—pink rectangular swath) for directional surface wave spectra; hurricane imaging RADiometer (HIRAD), scanning SFMR system now installed on NASA global hawk; airborne wind and rain atmospheric profiling radar, now a dual-frequency, dual polarized system for wind and rain 3D profiles from flight level to surface. A scanning Doppler lidar system has recently been added for wind profiling in clear air

atmospheric wind field above the sea surface by the tail-mounted, X-band Doppler radar operation in a fore-aft scanning mode. Details of this important technology is not included in this review.

Surface winds in hurricanes have been estimated remotely using the Stepped-Frequency Microwave Radiometer (SFMR) from the NOAA WP-3D aircraft for the past 31 years. Since the use of the GPS dropwindsonde system in hurricanes was first initiated in 1997 as a ‘gold standard’ for verifying and calibrating SFMR winds, routine collocated SFMR and GPS surface wind estimates have been made. During the 1998, 1999, and 2001 hurricane seasons, a total of 249 paired samples were acquired and compared.

The SFMR equivalent 1-min mean, 10-m level neutral stability winds were found to be biased high by 2.3 m/s relative to the 10-m GPS winds computed from an estimate of the mean boundary layer wind. Across the range of wind speeds from 10 to 60 m/s, the RMSE was 3.3 m/s. The bias was found to be dependent on storm quadrant and independent of wind speed, a result that suggests a possible relationship between microwave brightness temperatures and surface wave properties. Tests of retrieved winds’ sensitivities to sea surface temperature, salinity, atmospheric thermodynamic variability, and surface wind direction indicate wind speed errors of less than 1 m/s above 15 m/s.

For the first time, the NOAA/Aircraft Operations Center (AOC) flew Stepped Frequency Microwave Radiometers (SFMRs) on both WP-3D research aircraft for operational hurricane surface wind speed measurement in 2005. An unprecedented number of major hurricanes provided ample data to evaluate both instrument performance and surface wind speed retrieval quality up to 70 m/s (Saffir–Simpson category 5). To this end, a new microwave emissivity–wind speed model function based on estimates of near-surface winds in hurricanes by GPS dropwindsondes is proposed. For practical purposes, utilizing this function removes a previously documented high bias in moderate SFMR-measured windspeeds (10–50 m/s), and additionally corrects an extreme wind speed (>60 m/s) underestimate. The AOC operational SFMRs yield retrievals that are precise to within $\pm 2\%$ at 30 m/s, which is a factor of 2 improvement over the NOAA Hurricane Research Division’s SFMR, and comparable to the precision found here for GPS dropwindsonde near-surface wind speeds. A small (1.6 m/s), but statistically significant, overall high bias was found for independent SFMR measurements utilizing emissivity data not used for model function development. Across the range of measured wind speeds (10–70 m/s), SFMR 10-s averaged wind speeds are within 4 m/s (RMS) of the dropwindsonde near-surface estimate, or 5–25 % depending on speed. However, an analysis of eyewall peak wind speeds indicates an overall 2.6 m/s GPS low bias relative to the peak SFMR estimate on the same flight leg, suggesting a real increase in the maximum wind speed estimate due to SFMR’s high-density sampling. Through a series of statistical tests, the SFMR is shown to reduce the overall bias in the peak surface wind speed estimate by order 50 % over the current flight-level wind reduction method and is comparable at extreme wind speeds.

The updated model function is demonstrated to behave differently below and above the hurricane wind speed threshold (~ 32 m/s), which may have

implications for air–sea momentum and kinetic energy exchange. The change in behavior is at least qualitatively consistent with recent laboratory and field results concerning the drag coefficient in high wind speed conditions, which show a fairly clear “leveling off” of the drag coefficient with increased wind speed above ~ 30 m/s (Donelan et al. 2004; Powell et al. 2003). Finally, a composite analysis of historical data indicates that the earth-relative SFMR peak wind speed is typically located in the hurricane’s right-front quadrant, which is consistent with previous observational and theoretical studies of surface wind structure.

Recent studies (Dunion et al. 2003; Franklin et al. 2003; Powell et al. 1999, 2003) indicate that boundary layer models used to extrapolate flight-level wind speeds (Powell 1980; Deardorff 1972; Cardone 1969; Blackadar 1965) show a tendency to underestimate surface wind speeds >50 m/s. Anecdotal evidence also suggested that the SFMR underestimated surface wind speeds in similar conditions. Utilizing the previous GMF, comparisons of SFMR-derived wind speeds with GPS surface-reduced, 0–500-m layer-averaged winds indicated no such tendency (Uhlhorn and Black 2003), but, in fact, very few in situ data were available at speeds above 50 m s^{-1} . However, when compared with surface-adjusted lowest 150-m layer-averaged winds obtained in 2004, a low bias in SFMR retrievals became apparent at extreme wind speeds. With the recent surge in particularly intense hurricanes, analyzing and correcting this anomalous behavior has become critical. During 2005, a large dataset of contemporaneous SFMR and GPS dropwindsonde observations was obtained, resulting in significant improvement to the empirically derived SFMR emissivity–wind speed GMF, most notably at extreme wind speeds. This new model function has been implemented operationally on NOAA WP-3D SFMRs beginning in 2006, and on SFMRs installed on Air Force Reserve Command (AFRC) WC-130J aircraft since 2007.

The observation of a linear increase in sea surface emissivity with wind speed at hurricane force is a shift in our understanding of sea surface radiometric properties. In practical terms, the previous quadratic emissivity–wind speed model consistently underestimated winds at speeds >50 m/s, and the new linear GMF corrects this anomaly. From a scientific standpoint, additional evidence is found for a distinct physical change in the sea surface when surface winds exceed ~ 30 m/s, and further, that momentum and kinetic energy exchanges are relatively reduced at high wind speeds (Donelan et al. 2004). This gain in understanding may, potentially, lead to improvements in air–sea exchange parameterizations, ultimately resulting in superior hurricane intensity forecasts.

2.3 Tropical Cyclones, a Few Examples

In this section we describe a couple of special uses of microwave remote sensing that have benefitted TC understanding. These examples are in addition to the sequence about typhoon MEGI from 2010, that we cover with microwave observations that have become routine for real-time ascertaining of a TC’s size,

track and intensity. We discuss some particular uses of passive microwave, TRMM PR profiling, the sequence of scatterometer winds in the early stages of a TC, altimeter data used to assess heat content of the upper ocean in advance of a storm, the amazing looks of hurricane eyes seen with RADARSAT 1 SAR and last the climatology of total rainfall from landfalling TCs based on TRMM's long term record.

2.3.1 Multi-sensor Studies of TCs

The most advanced approach for obtaining quantitative data on tropical cyclones (and other marine weather systems) is the use of observations from several satellites by different sensors. These data are used extensively for both operational applications and for research on TC physics. An excellent source of multisensor data is a website developed at the Naval Research Laboratory Marine Meteorology Division (MMD), Monterey, California, USA: <http://www.nrlmry.navy.mil/TC.html> (see also Hawkins et al. 2001). Another source of multisensor data on tropical cyclones is a web site developed by the Earth Observation Research Center of the Japan Aerospace Exploration Agency: http://sharaku.eorc.jaxa.jp/TYP_DB/index_e.shtml where tropical cyclone data observed by TRMM's Precipitation Radar, TMI and VIRS, Aqua/AMSR-E and Midori-II (ADEOS-II)/AMSR are available for the period 1997–2011. The multisensor approach with a focus on microwave techniques is in ever-growing use. It was described in many papers devoted to estimates of particular parameters (wind, temperature, precipitation, etc.) and to diagnose and study structure and evolution of individual tropical cyclones. In particular, a novel morphing algorithm called the Morphed Integrated Microwave Imagery at the Cooperative Institute for Meteorological satellite Studies (CIMES) (MIMIC) was introduced by Wimmers and Velden (2007) to improve visualization of tropical cyclones, which in turn enhanced the ability to analyze and forecast these events. The authors' approach was to blend sequential individual microwave images together through a "morphing" process, which is the digital manipulation of two or more images to make them appear to change into one another naturally. Kidder and Jones (2007) developed a process for blending the total water vapor content values retrieved from the AMSU instruments on three NOAA satellites, and the SSM/I instruments on three DMSP satellites by application of the Alishouse (1990a) algorithm. The data are then mapped to a projection useful to forecasters and composited for 12 h to make a global map. These maps are produced hourly using Data Processing and Error Analysis System (DPEAS) software and made available to forecasters online. (See also papers by Hawkins et al. 2001; Knaff et al. 2011; Prasad and Singh 2007). Below two examples of multi-sensor study of tropical cyclones.

2.3.1.1 Tropical Cyclone Sinlaku (2008)

Typhoon *Sinlaku* developed as a tropical depression in the western Pacific Ocean, east of the northern Philippine Islands on September 8, 2008 and strengthened to a tropical storm the same day. The storm's outer rain bands intensified seasonal monsoon rains, causing flooding on the Philippine island of Luzon. On passing the Philippines, *Sinlaku* strengthened to become a typhoon and attained Category 4 status on September 10, 2008. Central pressure dropped sharply to 935 mb at 12 UTC on September 10 and in a day began to increase slowly and reached 945 mb at 12 UTC on September 13. Maximum sustained wind was around 50–64 m/s.

Results of *Sinlaku* sensing taken by satellite active and passive microwave instruments on September 10 are shown in Fig. 2.6. An Envisat ASAR image was acquired at 01:30 UTC. The *Sinlaku* eye looks as a dark circle due to weak winds. Its diameter is approximately 30 km. The light tone area surrounding the eye and elongated to the north marks the storm wind zone. Spiral rain bands of various length and width as well as individual rain cells appear as negative and sometimes positive radar contrast against the background (Fig. 2.6a). Magnitude and sign of the contrast depend on both the sea surface roughness and characteristics of the rain. In turn, rain falling on the sea surface can increase or decrease its roughness and also cause a decrease of radar signals due to twofold attenuation in the atmosphere.

MetOp ASCAT scatterometer data reveal the large-scale features of the sea surface wind field: large zones of cyclonic circulation to the north and to the south of *Sinlaku*, the increase of wind towards the typhoon center, wind shadows to the east of Luzon and to the south of Taiwan (Fig. 2.6b, c). The typhoon area is characterized by high values of the total water vapor content (Fig. 2.6e). Total cloud liquid water content exceeds 1–1.5 kg/m² in a large circular area around the center as well as in rain bands (Fig. 2.6f) in which heavy rains are typical. Strong attenuation by rain and clouds hinders wind speed estimates with the use of passive microwave measurements. As a result, AMSR-E retrieved wind fields cover only the areas with lower atmospheric absorption (Figs. 2.6d, g). The large-scale features of these fields agree well with the scatterometers data (Fig. 2.6b, c).

ENVISAT ASAR image of *Sinlaku* is seen in Fig. 2.7, which illustrates the fine details provided by this high performance SAR.

2.3.2 Altimeters and Upper Ocean Heat Content

A valuable application of altimetry in regard to TC research and operations has been the incorporation of altimetric data to estimate the depth of the warm water available as a heat source for hurricane intensification in the Caribbean and Gulf of Mexico region (Mainelli et al. 2008; Goni et al. 2009) and in the western Pacific ocean (Lin et al. 2008). Assimilation of altimeter data into operational oceanographic models and the increased precision (of the order of 1 cm in sea surface height), makes this

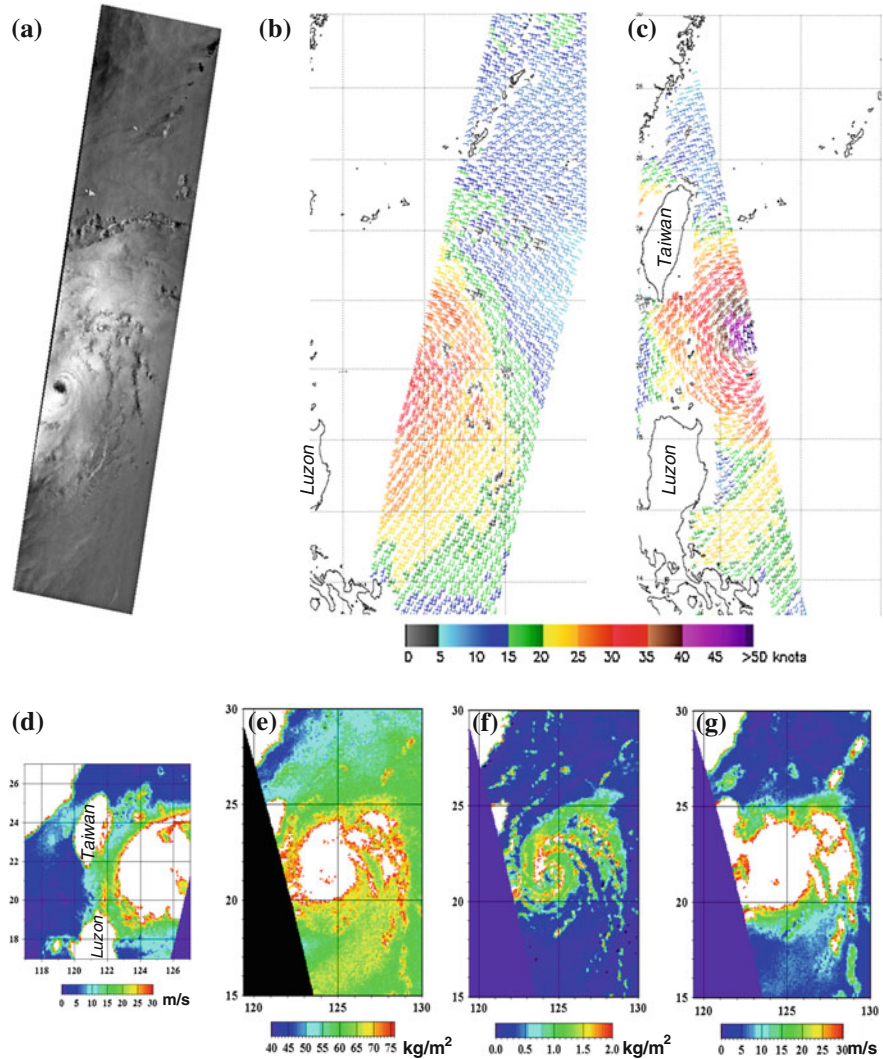
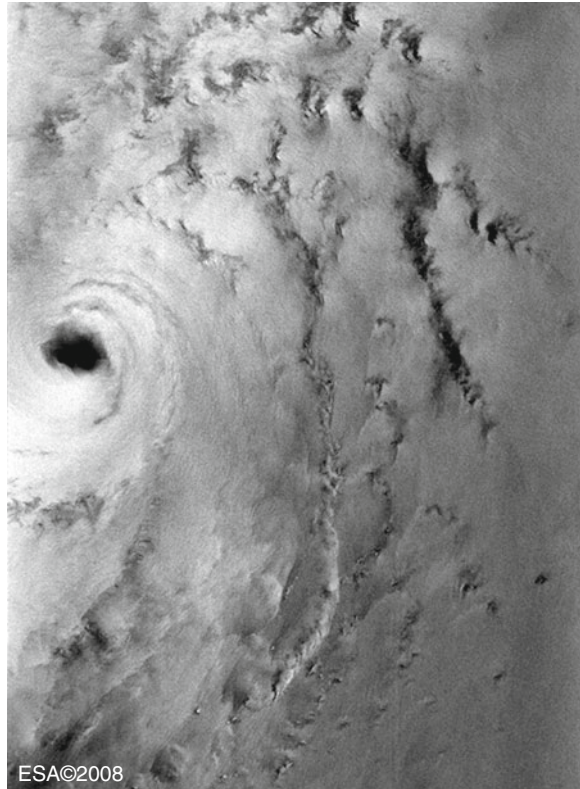


Fig. 2.6 Typhoon Sinlaku sensing by active and passive microwave sensors: Envisat ASAR image at 01:30 UTC (a), wind field derived from MetOp ASCAT at 01:37 UTC (b) and at 12:43 UTC (c) and from Aqua AMSR-E at 17:50 UTC (d) on 10 September. Fields of total atmospheric water vapor content (e), total cloud liquid water content (f) and wind speed (g) retrieved from Aqua AMSR-E measurements at 04:45 UTC on 11 September 2008

technology ready for operational use. EUMETSAT and NOAA have already established cooperation agreements with regard to altimetry. The method for using altimeter data when estimating the heat content in warm eddies ahead of the arrival of a TC, includes assimilation of the altimeter information into a numerical model of the upper ocean, which has been initialized with buoy data of the temperature structure as

Fig. 2.7 Spiral rain bands converging to Sinlaku eye on Envisat ASAR image acquired on 10 September 2008 at 01:30 UTC



a function of depth, which is not obtainable from space. Buoys may have to be placed in strategic locations by aircraft deployment, but this is well worth the expense, as was proven in the case of the Katrina hurricane, which was well predicted, including its intensification before landfall as it travelled across a warm eddy.

Figure 2.8 shows warm eddy in the Gulf of Mexico, revealed by altimeter measurements in conjunction with upper ocean model and initialization from in situ measurements. TC Katrina intensity levels as it passes over this eddy is illustrated with the size and color of the circles along the track.

2.3.3 SAR Observed Eyes of Hurricanes

The SAR of RADARSAT 1 and 2 is only 500 km wide in the so-called wide mode sampling. That means that it will not often observe a whole TC within its swath. Further, the Canadian Space Agency's agents, who operated the satellite sampling, needed requests for taking an image many days in advance of the satellite passing

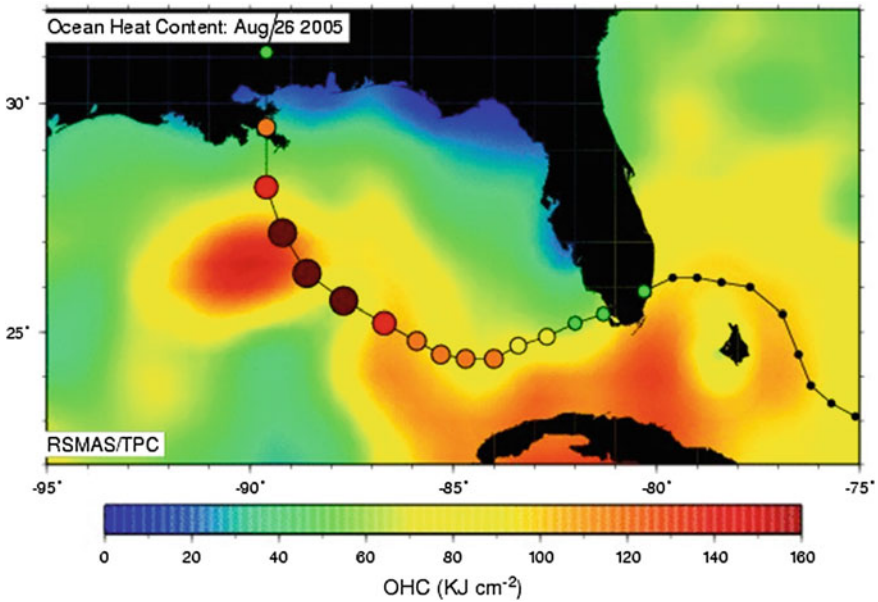


Fig. 2.8 Ocean heat content (OHC) for Hurricane Katrina used to derive OHC input to the statistical hurricane intensity prediction system (SHIPS) used operationally at the U. S. National Hurricane Center (NHC). Track of hurricane Katrina across the Gulf with *dots* a TS, *green* CAT1, *yellow* circles CAT2, *tan* CAT3, *red* CAT4 and *dark brown* CAT5. Rapid intensification began just after crossing the loop current boundary outlined in ocean heat content (OHC) from satellite altimeters as *yellow*, with deep *red* indicating a warm ring in the process of breaking off and moving westward in the Gulf. It is the movement away from this warm ring and onto the shallow, relatively cool shelf waters that accompanies Katrina's rapid weakening (Mainelli et al. 2008)

the desired location. Fortunately, smart operators pushed the button to take images of hurricane Mitch at category 5 in the Caribbean in the early days of RADARSAT 1 operations. A wonderful development followed in that the Canadian Space Agency developed a program called *Hurricane Watch*, in which the long lead times were waived and operators were able to catch the centers of many TC's (e.g. Iris and Burger 2004; Vachon et al. 2001). These images are haunting and interesting, but full interpretation of what exactly a SAR observes from space in high wind and heavy rain situations is not yet achieved. The images of TC eyes obtained during 3 hurricane season in Fig. 2.9 clearly show that the vortex may be distorted in ways that indicate mesoscale circulations or breakdown of the vortex.

Such features had been suspected in studies of damage on land, where the damage was higher in streak-like regions (Black, personal communication), which would be consistent with the higher wind speeds where a mesoscale circulation was added to the vortex wind speed. Breakdown of vortices have been found in laboratory and theoretical studies and similar features can sometimes be seen in visible images from geostationary satellites (Schubert et al. 1999; Kossin et al. 2002; Kossin and Schubert 2001, 2004; Montgomery et al. 2002).

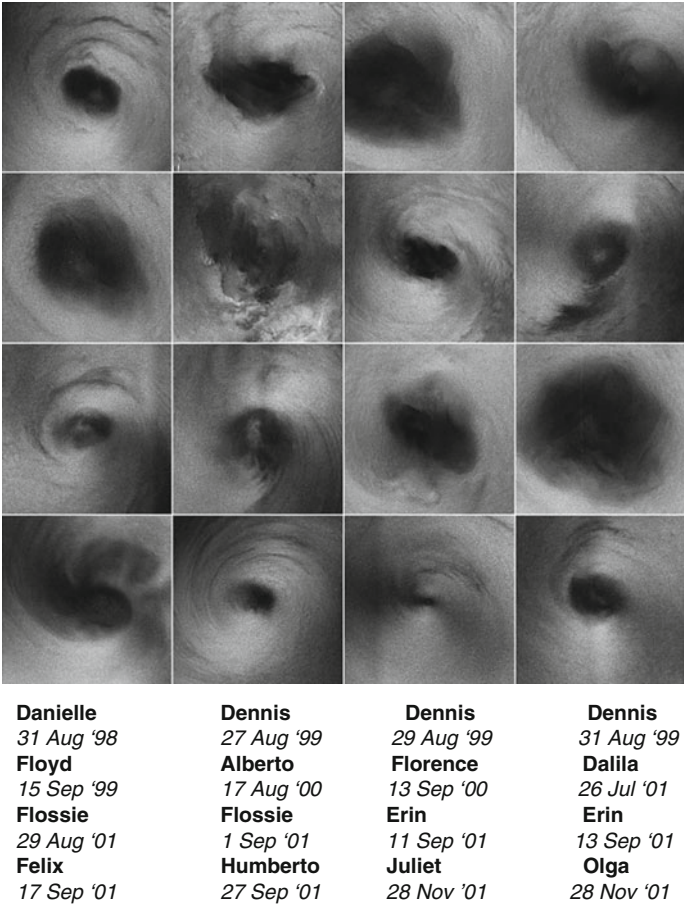


Fig. 2.9 RADARSAT-1 SAR images of hurricane eyes (after Vachon et al. 2001) (© CSA, 1998, 1999, 2000, 2001)

2.3.4 Climatological Information on Precipitation From TRMM

A nice example of using TRMM’s algorithms calibrated by its own rain radar and coastal radars is found in the climatological study of rainfall in tropical cyclones by Lonfat et al. (2004). The authors collected data from TRMM’s TMI on precipitation associated with TC’s for a 3 year period, January 1, 1998–December 31, 2001. They divided the 2121 instantaneous precipitation observations into 3 levels of storm intensity, tropical storm, Category 1–2 and 3–5 and separated the data for 6 ocean basins. They evaluated the precipitation in 10 km wide annuli around the storm center, out to a radius of 500 km, although in the outer regions their

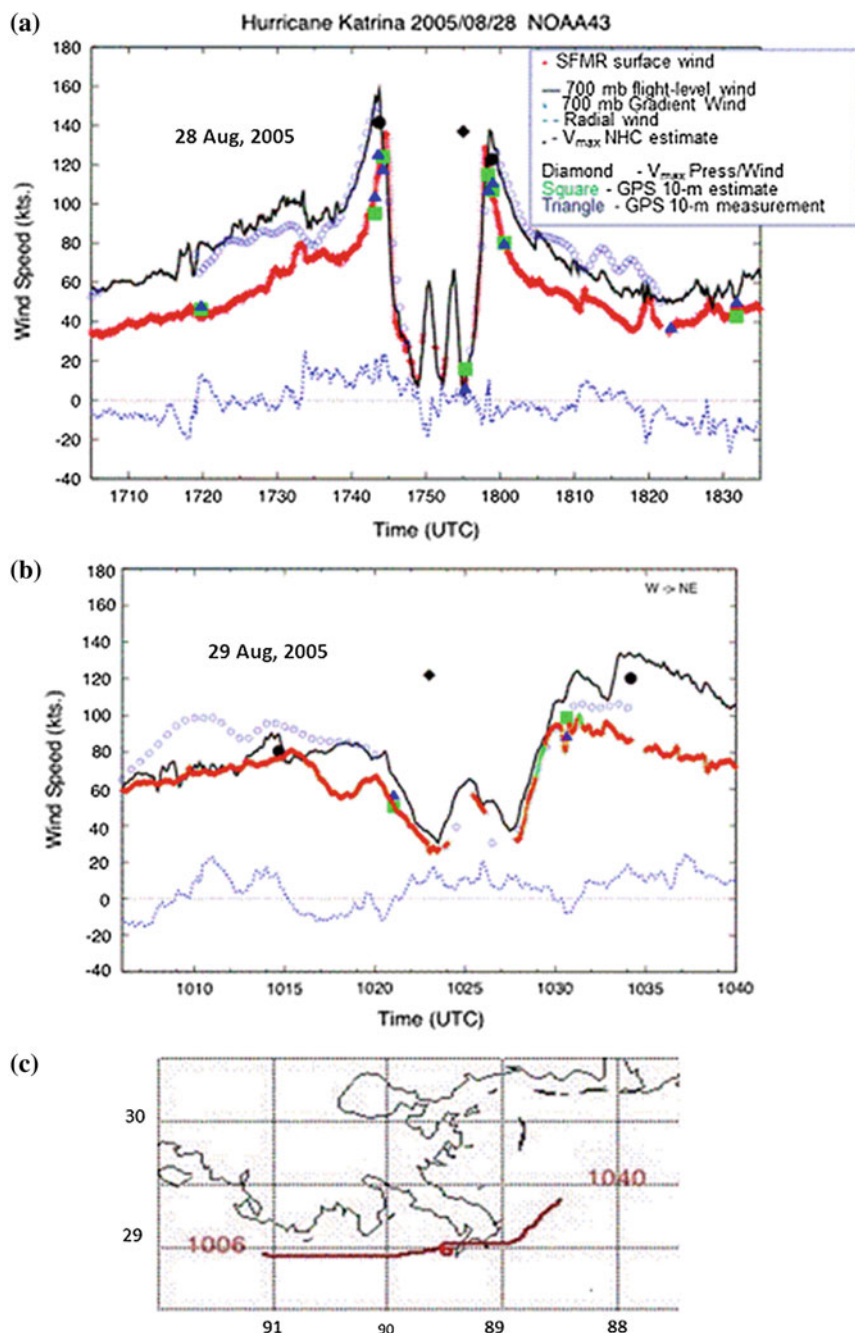
statistical sample was often too small due to the narrow swath of TMI. The study gave information about the asymmetry in the rainfall with respect to the storm track and as a function of storm intensity. They could calculate the total precipitation associated with each type of storm over its track. The data can be used to predict the rain falling on land after landfall and improve flood-risk forecasting. This subject has come a long way thanks to TRMM, which points the way to the next planned system described in [Sect. 2.5](#). Stephens and Kummerow (2007) discuss the improvements in estimates that are possible when clouds and precipitation are analyzed in concert using CloudSat and TRMM information.

2.3.5 Airborne Passive Microwave Observations of TCs

As hurricane Katrina approached landfall in the state of Louisiana, USA, on August 28, 29 of 2005, the US instrumented aircraft, operated by the US Air Force for reconnaissance and for the Hurricane Research Division (HRD) of NOAA in Miami for both reconnaissance and research, were flying their characteristic patterns through the eye of this storm. It was a category 5 storm off shore with highest winds of 142 kt, but fortuitously the intensity declined to a category 3 just before landfall with surface winds estimated at 100 kt. [Figure 2.10](#) is a display of the flight tracks, the estimated surface winds along the flight track by the SFMR on the HRD aircraft and by reduction of flight level winds at 700 mb to the surface from the W 3 130. Dropsonde wind speed estimates applying to 10 m height are also seen in these two figures. All 3 surface wind speed estimates show general agreement. Gridded wind fields based on these two data sets are also generated by the HWIND computer program operated by HRD and provided to the hurricane forecasters in near real time ([Fig. 2.10e, f](#)). The wind fields are similar, but there are also differences, even though the two wind fields apply at the same time. This indicates that the use of surface measurements with the SFMRs is desirable, but that inter-comparisons and calibration efforts must continue.

2.4 Applications of Microwave Remote Sensing to Typhoon MEGI

Two of the authors of this chapter (LM and KK) experienced the outer regions of super typhoon Megi during the 2010 Pan Ocean Remote Sensing Conference (PORSEC), while in Keelung, Taiwan, during October 18–23, 2010. In particular, heavy rains in the northeast of Taiwan, on the Philippines and in China were connected with Megi. 45 persons died, 28 went missing. There were numerous landslides, roads and power lines were destroyed, the crop damaged, etc. General economic damage reached approximately 611 million US\$. Several rainy days in



◀ **Fig. 2.10** WP-3D observations along west to east flight tracks in Hurricane Katrina on 28 and 29 August, 2005 (panels **a** and **b**), respectively, near peak intensity on the 28th and just prior to landfall on the 29th. Profiles of observed 700 mb wind and gradient wind speed computed from smoothed D-value (pressure minus radar altitude difference) profiles and SFMR surface wind speed. Also shown for comparison are dropsonde measured 10-m wind speeds, dropsonde estimated 10-m wind speeds (from mean boundary layer winds), NHC peak wind estimate (*black solid circles*) and NHC peak wind from pressure-wind relationship (*black diamond*). Panel **c** is the west to east flight track, just offshore, on the 29th. **d–g** H*WIND surface wind analysis centered on 0930 GMT 29 August. Panel **d** indicates analysis of surface wind estimated as 80 % of 700 mb flight-level measurement and panel **e** indicates surface wind analysis from SFMR surface wind measurements. Contours are in 5-kt intervals with *yellow–brown* transition indicating 50 kt and *red–magenta* transition indicating 90 kt. *White arrows* are estimated surface wind direction (flight level wind direction minus 25°). Panel **f** is the flight track and estimated surface wind barbs for the WC-130H aircraft flying at 700 mb and **g** is the WP-3D 650 mb flight track and surface wind barbs. Additional surface wind observations are indicated by the legend between panels

Keelung were caused by a spiral rain band of the typhoon. All participants of the conference watched *Megi*'s track every day. Moreover, the Internet allowed us to routinely obtain the data about *Megi* from several satellites: Aqua, Terra, TRMM, MetOp, Envisat and others which were processed with the use of both official and our original algorithms. These observations and ancillary information were included in the reports which were presented at a tropical storm session during PORSEC 2010. Research was continued in Russia by LM. This work, which has allowed a detailed quantitative description of *Megi* evolution is in part presented below. Fortunately, a joint field program between the University of Taiwan and U.S. agencies (WHICH) was carried out in the South China Sea, using aircraft, ships and buoys during this same period. This program had as its goal to understand the structure and evolution of typhoons in this area and the influence of sea surface temperature patterns and upper ocean structures. One of us, PB, was in the field in charge of the aircraft program, and has been able to select representative examples of microwave and other observations from the aircraft for the same period of time.

2.4.1 *Megi Observed From Space*

The Japan Meteorological Agency (JMA) marked a developing area of low pressure located southeast of Guam as a tropical depression on October 13. Early on that day, the Joint Typhoon Warning Center (JTWC) in Hawaii also classified the system as a tropical depression, giving it the identifier 15 W. Sea surface temperature exceeding 28 °C and high ocean heat content contributed greatly to strengthening of the depression. The low pressure system situated to the southwest of a subtropical ridge slowly tracked west-northwest towards the Philippines. Around 1200 UTC, the depression further intensified into a tropical storm, earning the name *Megi* from the JMA (Fig. 2.11).

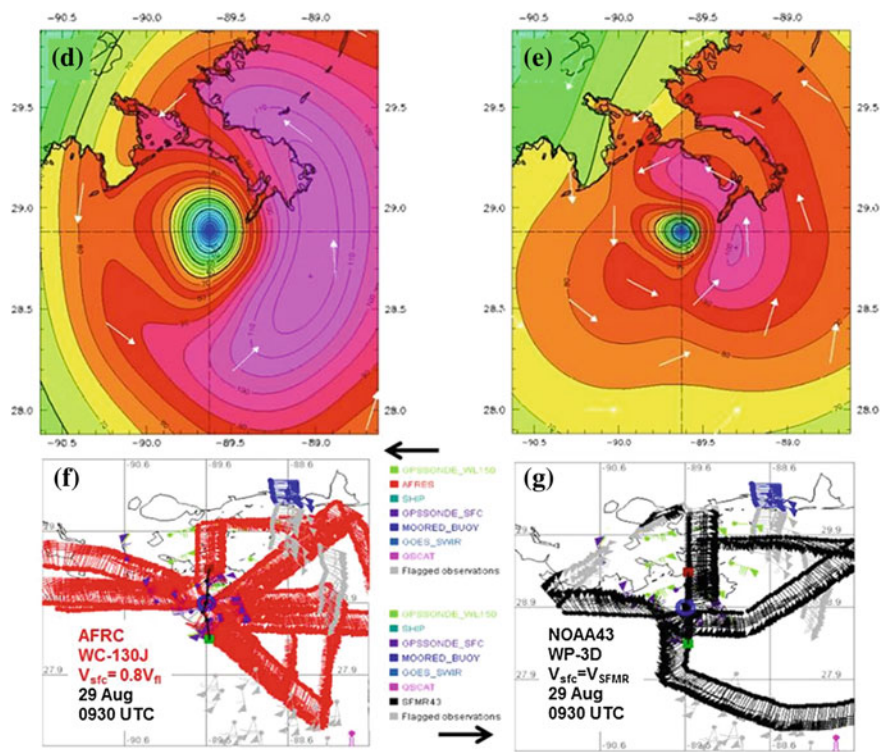


Fig. 2.10 continued

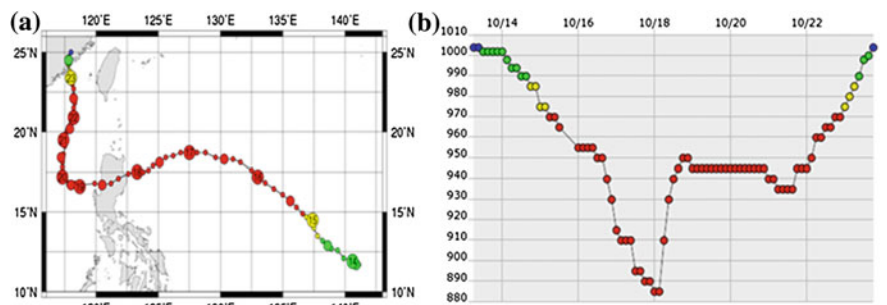


Fig. 2.11 Track (a) and central pressure (b) in super Typhoon Megi. The colors represent: blue tropical depression; green tropical storm; yellow severe tropical storm and red typhoon (<http://agora.ex.nii.ac.jp/digital-typhoon/help/track.html.en>)

Throughout the morning of October 14, satellite visible and infrared images showed that a dense overcast developed over the center of *Megi*. Later that day, an eye appeared on satellite imagery, resulting in the JTWC upgrading *Megi* to a

minimal typhoon. *Megi* progressed northwestward around the periphery of the subtropical ridge, strengthening to a category 3 typhoon on October 16. Later in the day, the storm turned westward, and strengthened to a category 5 on the Saffir-Simpson Scale for Hurricane Classification (Table 2.6). *Megi*'s cloud system consisting of well-developed spiral rain bands, a central circular dense cloud patch with a cloudless eye covered a large area to the east of Taiwan and Luzon (Fig. 2.12a). Measurements were obtained on 17 October at 04:55 UTC when central pressure dropped to 910 mb. The wind field derived from the Aqua AMSR-E microwave brightness temperatures with the use of an algorithm by Mitnik and Mitnik (2010, 2011) is shown in Fig. 2.12b. Rains and heavy clouds prevent wind speed retrieval in the areas marked by white color in Fig. 2.12b.

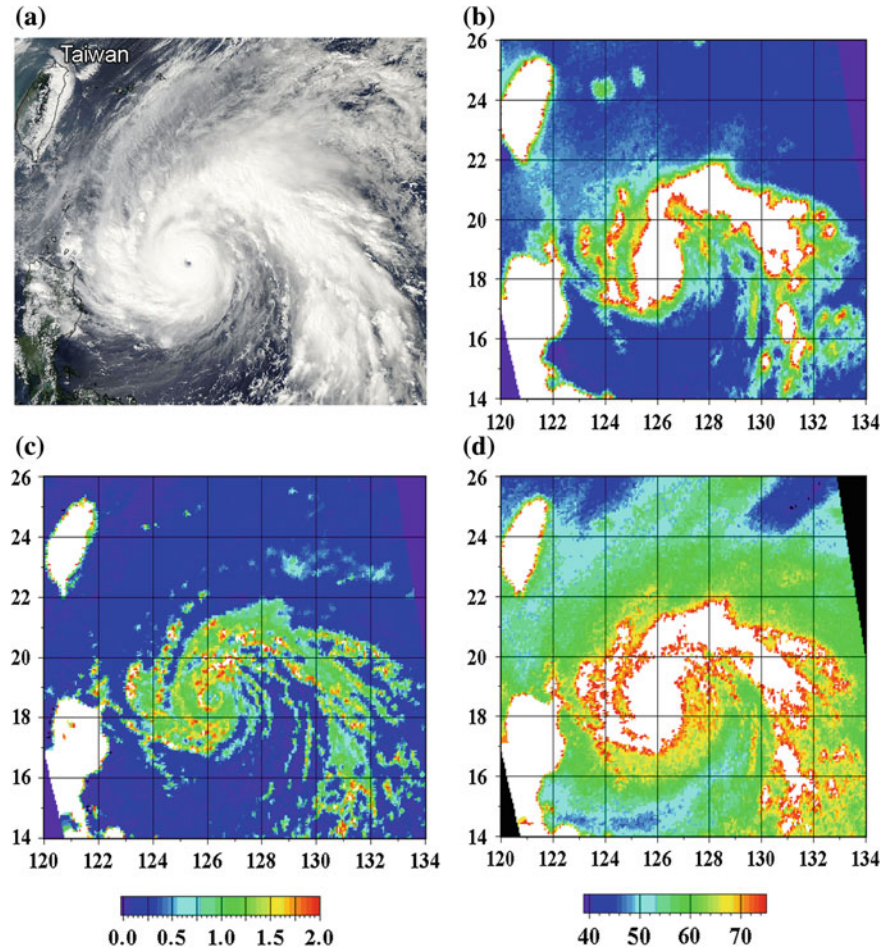


Fig. 2.12 Aqua MODIS visible image (a), Aqua AMSR-E-derived wind speed (b), total cloud liquid water content (c), and total water vapor content (d) obtained on 17 October at 04:55 UTC

The total cloud liquid water content Q and total water vapor content V in the typhoon area derived with the use of an algorithm by Mitnik and Mitnik (2003), Mitnik et al. (2009), and Bobylev et al. (2010) are shown in Fig. 2.12. A circular eye wall with a diameter of approximately 100 km and rain bands with $Q > 1.5 \text{ kg/m}^2$ are clearly seen in Fig. 2.12c. The width of the eye wall is approximately 20 km. Within the eye, Q values decreased to 0.5 kg/m^2 and even lower. An area with high water vapor content ($55\text{--}65 \text{ kg/m}^2$) surrounds the cloud field (Fig. 2.12d). V -values became still higher closer to heavy clouds and precipitation. V and Q retrieval errors are also higher here.

Satellite SAR images possess high spatial resolution. Typhoon Megi was within an Envisat ASAR swath on 17 October at 01:22 UTC (Fig. 2.13a). The brightness distribution of a SAR image of a tropical cyclone gives a detailed picture of the surface roughness which is determined mainly by the sea surface wind speed and direction and also rains since rain drops falling on the sea surface change its roughness characteristics.

Besides, heavy rains that are typical for eye wall and spiral bands of typhoons produce significant attenuation of SAR signals propagating from satellite to the sea surface and back from the sea surface to the satellite. An enlarged fragment of the image (Fig. 2.13b) shows the structure of the eye, eye wall and narrow bands spiraling to the eye. They appear with negative radar contrast against the background. The darker bands and patches with irregular edges (Fig. 2.13c, d) are indicators of the rain-induced two-way attenuation as well as sea surface roughness damping (Lines of squalls which frequently accompany heavy rains from convective clouds manifest themselves as narrow bright lines, Fig. 2.13e).

On 17 October Megi continued to strengthen. The central pressure decreased to 890 mb, maximum wind increased to 125 knots, the largest radius/diameter of storm wind was 220/440 km, and the largest radius/diameter of gale force wind reached 650/1,060 km. Current satellite sensors cannot estimate so strong winds due to physical and technical limitations. Maximum estimated winds derived from MetOp ASCAT data over the Megi central area did not exceed 25–27 m/s (Fig. 2.14).

However, currently airplane Stepped Frequency Microwave Radiometer (SFMR) has measured wind speeds up to 70 m/s in Atlantic tropical hurricanes (Uhlhorn et al. 2007). In Northwest Pacific typhoons SFMR-derived wind speed was 92 m/s—the highest SFMR wind ever measured. Figure 2.15 shows SFMR wind speed and rain rate retrievals as well as flight level wind versus *Megi* radius.

Table 2.6 Saffir–Simpson scale for hurricane classification

Strength	Winds (kts)	Pressure (mb)	Storm surge (m)	Damage
Cat. #1	65–82	>980	1.2–1.5	Minimal
Cat. #2	83–95	965–979	1.8–2.5	Moderate
Cat. #3	96–113	945–964	2.7–3.6	Extensive
Cat. #4	114–135	920–944	4.0–5.5	Extreme
Cat. #5	>135	<920	>5.5	Catastrophic

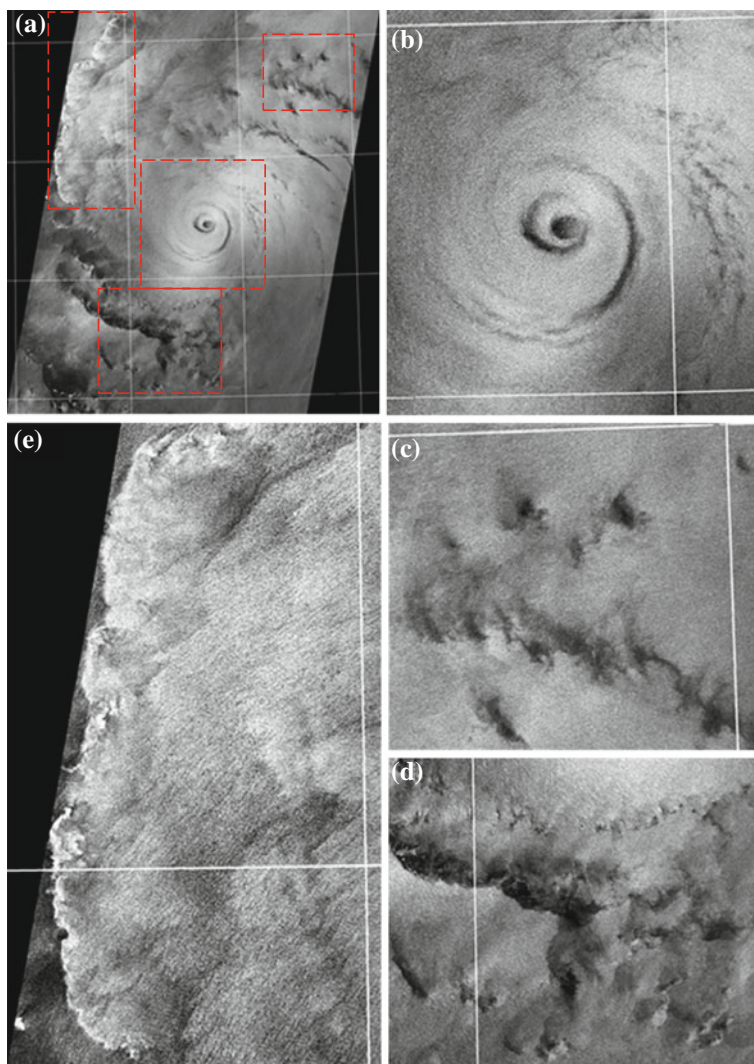


Fig. 2.13 Envisat ASAR image of typhoon Megi acquired on 17 October at 01:24 UTC (a) and enlarged fragments showing the signatures of eye and eye wall (b) rain cells and spiral rain bands near the wall (c) and (d) and squall lines (e). Red dotted rectangles in (a) mark the fragment boundaries (ESA©2010, ESA©2008)

Airborne SFMR observations were carried out at NE-SW pass across the *Megi* center on 17 October at 11:00–11:34 UTC. Wind speed reached 88 m/s and rain rate—40 mm/h.

On October 18, 2010, central pressure dropped to a minimum value of 885 mb. At approximately 07 UTC, the center of *Megi* crossed Luzon (Philippines) and continued westward movement. Central pressure began to rise and at 18 UTC

Fig. 2.14 MetOp ASCAT-derived wind field in typhoon Megi area on 17 October at 13:15 UTC when central pressure dropped to 895 mb. Color scale is wind speed in knots

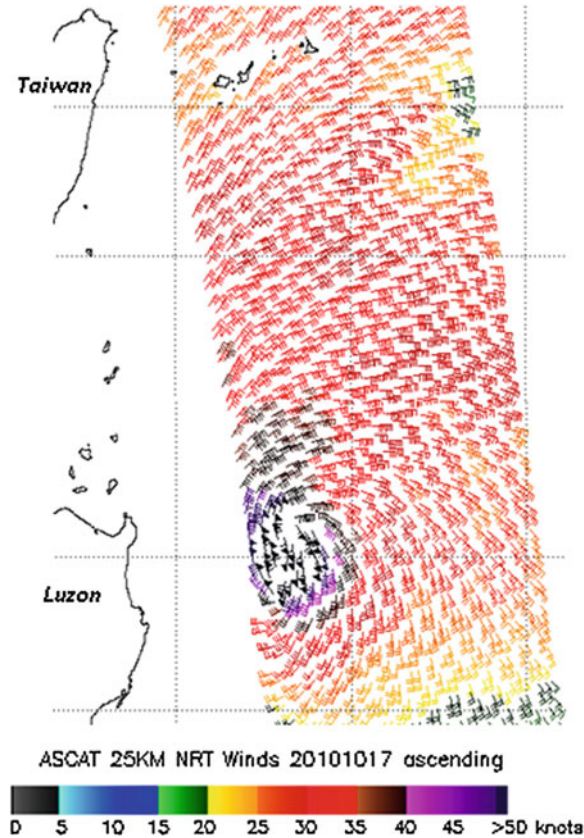
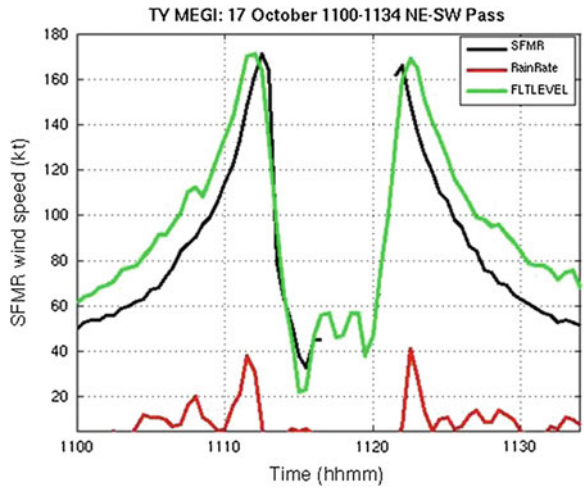


Fig. 2.15 Surface (*black*) and flight level (*green*) wind measured on October 17 during a traverse of super Typhoon Megi by the WC-130J aircraft using the stepped frequency microwave radiometer (SFMR) and flight level wind sensors. Vertically integrated rain rate (*red*) is also observed by the SFMR



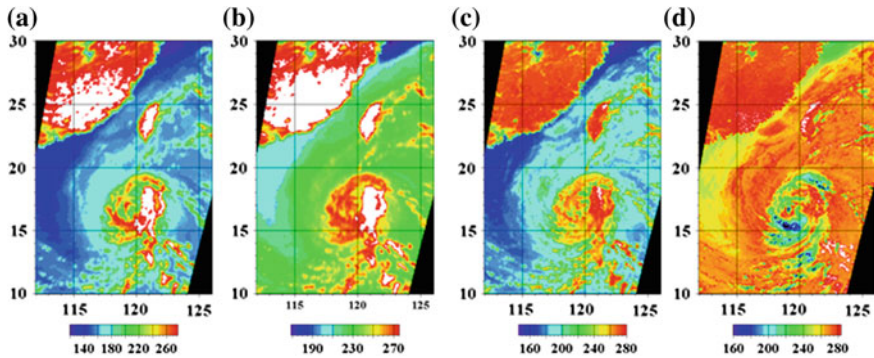


Fig. 2.16 Aqua AMSR-E brightness temperatures in Kelvin degrees of typhoon Megi at 18.7 GHz, H-pol (a), 23.8 GHz, H-pol (b), 36.5 GHz, H-pol (c) and 89.0 GHz, H-pol (d) measured on 18 October at 17:50 UTC

reached 950 mb. AMSR-E brightness temperatures at frequencies of 18.7, 23.8, 36.5 and 89.0 GHz with horizontal (H) polarization measured at 1750 UTC are shown in Fig. 2.16. A dark arrow marks the CloudSat track.

CloudSat's Cloud Precipitation Radar (CPR) operating at a frequency of 94 GHz and viewing in nadir crossed the eastern sector of the typhoon on a North–South track approximately when the *Megi* center was located over Luzon and central pressure increased to 945 hPa. CPR shows clouds at elevations higher than 16 km (Fig. 2.17). The blue areas along the top of the clouds indicate cloud ice. The wavy blue lines on the bottom center indicate intense rainfall. Where the solid line along the bottom disappears there is intense rainfall exceeding 30 mm/h. (<http://esciencenews.com/topics/astronomy.space>).

A moisture-saturated cloud band crossed Northern Taiwan (Fig. 2.18) and gave rise to torrential rains.

After traversing Luzon, the typhoon weakened to a category 2 but rapidly regained strength in the South China Sea where SST exceeded 30 °C, strengthening back to a category 4 on October 19. The eye diameter increased to approximately 120 km (Fig. 2.19). The circular eye wall had high contrast at all AMSR-E channels due to intense precipitation and high values of cloud liquid water content, Q . From analysis of brightness temperatures it follows that Q values exceeded 1.5–2 kg/m² in the eye wall and were less than 0.3–0.4 kg/m² inside the eye.

Megi slowed its forward speed due to the arrival of another trough over the South China Sea extending over the Taiwan Strait and breaking the ridge, turning the typhoon northwestward, then towards the north–northeast.

On 21 October *Megi* was observed by satellite SAR, Fig. 2.20. This time it was the German Aerospace radar satellite TerraSAR-X (http://www.dlr.de/en/desktopdefault.aspx/tabid-1/86_read-27445/). The swath width of TerraSAR-X is 100 km. The size of the dark central area (eye of *Megi*) is approximately 50 km, confirmed by Aqua AMSR-E and MODIS data, Fig. 2.20 and also by Fig. 2.21,

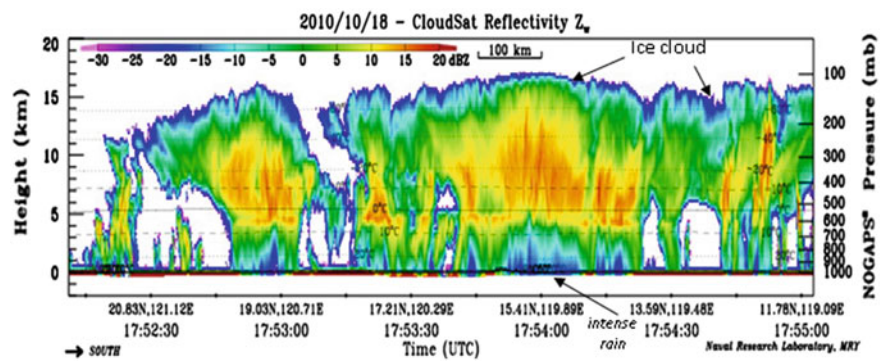


Fig. 2.17 CloudSat reflectivity of typhoon Megi cloudiness on 18 October at 17:54 UTC. The cloudsat precipitation radar (CPR) operating at a frequency of 94 GHz and viewing in nadir crossed the eastern sector of the typhoon on a North–South track at approximately when the Megi center was located over Luzon and central pressure increased to 950 mb. CPR shows clouds at elevations higher than 16 km. The *blue areas along the top of the clouds* indicate cloud ice. The *wavy blue lines on the bottom center* indicate intense rainfall. They cause strong attenuation of 94-GHz radar signals. When rainfall exceeds approximately 30 mm/h radar signals reflected by the sea surface disappear due to high two-way attenuation

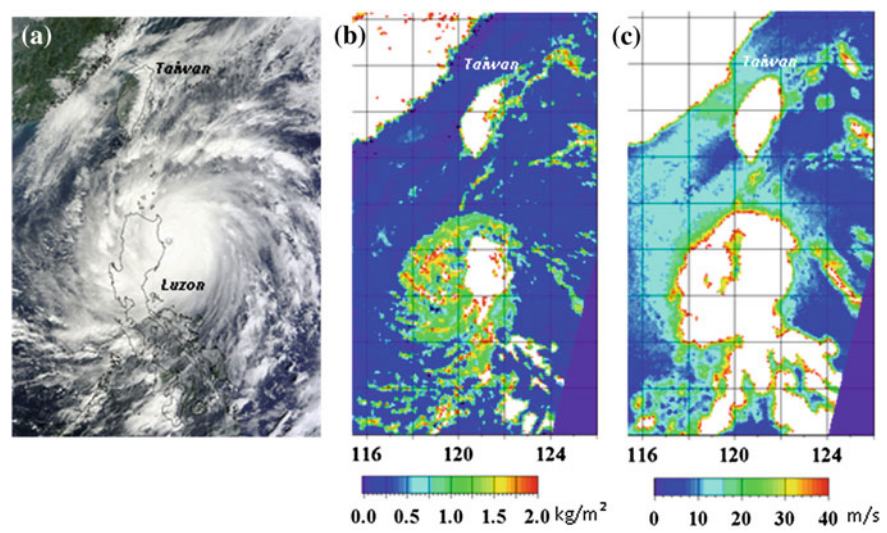


Fig. 2.18 Aqua MODIS visible image at 02:35 UTC (a), Aqua AMSR-E-derived total cloud liquid water content (b), and wind speed (c), at 17:38 UTC on 18 October, 2010. AMSR-E TBs allow retrieval of the cloud liquid water content and total water vapor content over the ocean and when rain rate is less than approximately 5 mm/h. That is why Taiwan, Luzon and China are shown by *white color*

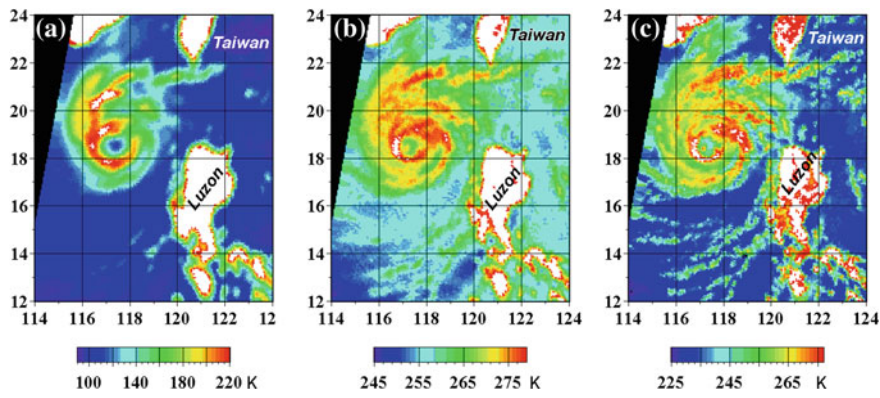


Fig. 2.19 Aqua AMSR-E brightness temperatures in Kelvin degrees taken on 20 October 2010 at 17:38 UTC and used in wind speed retrieval algorithm: (a) 10.7 GHz, H-pol; (b) 23.8 GHz, V-pol and (c) 36.5 GHz, V-pol. Central pressure $P_{\min} = 948$ mb, $V_{\max} = 100$ knots

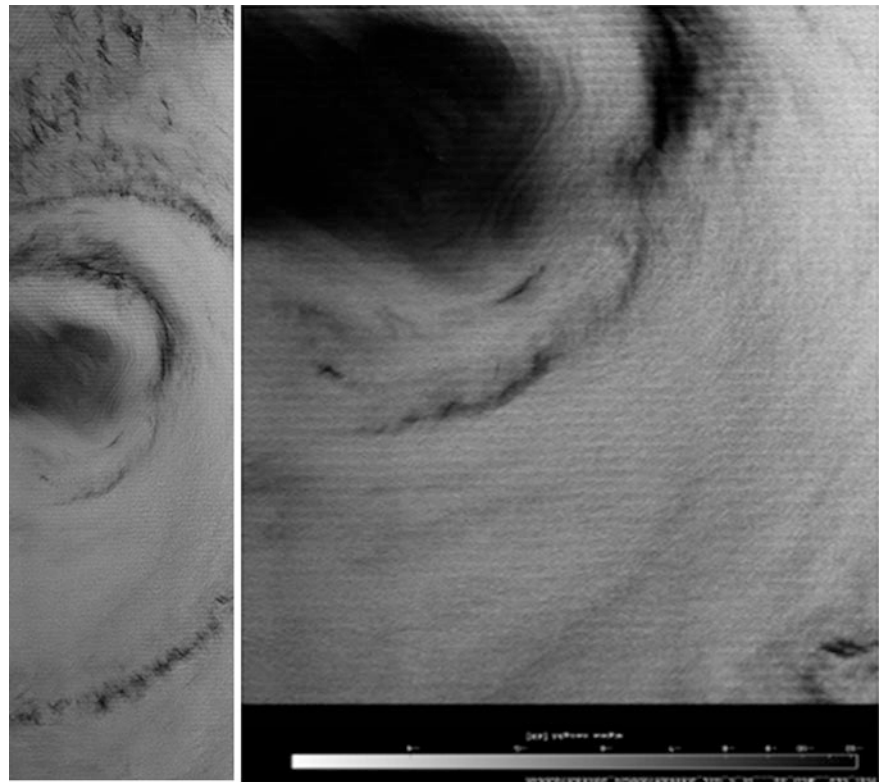


Fig. 2.20 TerraSar-X image of typhoon Megi at 22:06 UTC on 21 October 2010 over the Northern South China Sea. Pixel size of the ScanSAR mode is 8.25 m. Swath width is 100 km, and the scene covers a distance of 450 km (*left*) http://www.dlr.de/en/desktopdefault.aspx/tabid-6221/10233_read-27445/. The radiometric calibrated image (*right*) (from Lehner et al. (2011))

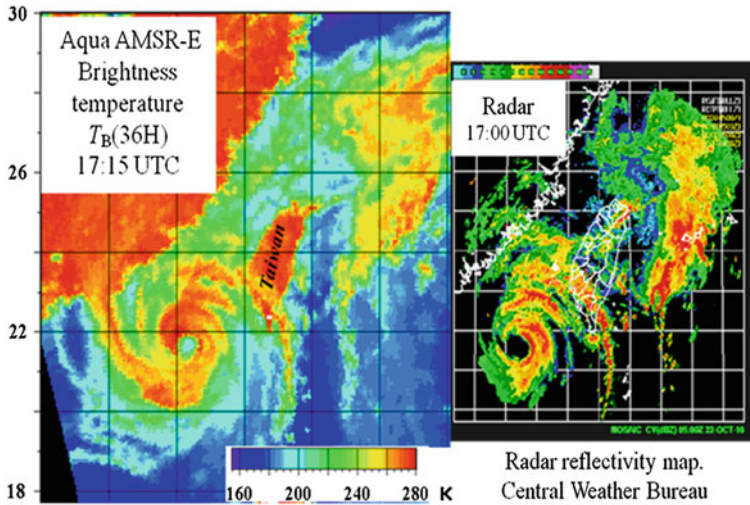


Fig. 2.21 Aqua AMSR-E brightness temperature at 36.5 GHz with horizontal polarization acquired at 17:15 UTC and radar reflectivity map produced by coastal radars of the Central Weather Bureau in Taiwan at 17:00 on 22 October 2010 (b)

whose times of capture enclose the TERRA-SAR image. It is significantly smaller than in an earlier image (Fig. 2.19), while the central pressure decreased only by 5 mb (See Fig. 2.11). Dark curvilinear bands and patches are due to scattering of 3-cm radiation by water droplets and hail.

On 22 October a Taiwan coastal radar traced *Megi*'s northward movement and changes in its spiral rain bands. The field of brightness temperature measured by Aqua AMSR-E and a radar reflectivity map acquired with a time difference of 15 min are in a good agreement, since both satellite and ground sensors are sensitive to water droplets in the atmosphere (Fig. 2.21).

Satellite measurements obtained by passive and active sensors prove their usefulness for quantitative research on the life cycle of tropical cyclones and for operational applications especially in data sparse areas. This was demonstrated by quasi-operational analysis of near real-time satellite data obtained over *Megi*, provided via the Internet and presented during PORSEC2010 in Keelung. Microwave sensors enhance overall knowledge and understanding of TC evolution, and can significantly improve forecasts of their tracks and intensity, as well as, dangerous terrain effects such as storm surges, heavy precipitation and flooding.

2.5 Summary and Perspectives

Over the past 4 decades remote sensing has developed to include passive and active microwave instruments, employing a wide range of frequencies and sampling techniques. Applied to TC research and operational diagnosis this work has

had very significant impact. Together with frequent observation in the visible and infrared spectrum from geostationary and polar orbiting satellites, they have allowed new insights and development of theory and numerical models. Improvements in understanding of TC structures and their life cycle and in understanding the interactions of the microwave signals with the underlying sea surface and the atmospheric constituents have ensued—One might ask, where can we best go from here?—Much work is still needed for understanding the TC life cycle, especially rapid intensification. Economic stress has slowed down the replacement of many valuable sensors as they fail of old age. The enterprise of satellite remote sensing (and aircraft remote sensing as well) is an expensive undertaking, but not with the perspective of the disasters that occur, when coastal populations are attacked unawares by intense TC's. Such events were recorded especially before the satellite era (e.g. the New England storm of 1938, Galveson Texas, 1900 and 1915). Pielke and Landsea (1998) review the cost of the 14 most expensive hurricanes up to 1998 with normalization based on inflation, population density and level of wealth that has changed over time. The cost has kept on rising, but the loss of life has been dramatically reduced when the populations are warned and evacuated. Hurricane Katrina's impact on Louisiana in 2005 was largely due to infrastructure failures and improper evacuations. The approaching hurricane and its intensity were known. In no region on the globe should surprises like the Galveston 1900 hurricane and the *Katrina* disaster happen today, but communicating the risks to the threatened populations and having transportation and shelters prepared can still be a problem.

For global watchfulness from space we need dependable, operational satellite systems with frequent sampling. This will require full international cooperation from inception of design and orbit planning, through development, operations and data distribution (Katsaros et al. 2011). Such data must be made available in near real time for optimal reward in improved warnings. In order to accomplish this in greater measure than we have today, scientists, politicians and institutional leaders must consider this holistic, international approach a priority. The uncertainty of research results, when observations remain punctual, and conclusions *per force* are anecdotal makes it difficult to gather folks into action and achieve adoption of good risk-aversion practices. It is, therefore, crucial to lay a solid foundation of high quality, routine and relevant data for the hoped-for international cooperation. Several international organizations are at work on these principles, notably the World Meteorological Organization (WMO) and various branches of the United Nations Educational, Scientific and Cultural Organization (UNESCO). The UNESCO efforts include education and training for capacity building in many countries where the need for better science training exists.

All along creative minds present us with new and innovative ideas for how to improve the measurements and the use of the information. Examples of sophisticated new systems include the scanning altimeter, Surface Water and Ocean Topography (SWOT, Fu et al. 2009; <http://swot.jpl.nasa.gov/>). Satellite altimetry is recognized as an essential component of the Global Earth Observation System of Systems. To date satellite altimetry has focused on the open ocean (Fu and

Cazenave 2001), but the coastal ocean has emerged as an important domain for these data. Only through a synergy from various altimeters can a thorough and complete characterization of mesoscale circulation be obtained. Coastal and mesoscale issues have gotten a new push with the proposed SWOT, which would provide better coverage by an altimeter system than the current nadir viewing ones. It would also have multiple frequencies providing better accuracy.

For the precipitation and water content, as vapor or cloud liquid water in storms of all kinds, a follow-on system to TRMM has been proposed, which would include many passive radiometers and a central rain radar to provide the inter-calibration; the Japanese Aerospace and Exploration Agency, JAXA, and NASA are playing important roles with other international partners included. A US National Research Council Report describes the GPM mission with focus on NOAA's role.

We could increase the revisit time of sampling the ocean surface wind readily, if all nations making scatterometer measurements coordinated their equator crossing times. Liu et al. (2008b) provide graphic illustration that 6 h revisits or better would be possible globally with 4 scatterometers, if orbits are ideally timed, but even two coordinated scatterometers already improve chances of catching circulation patterns during early developments of tropical depression within 12 h (even though many systems with early circulations do not develop to storms; see Liu et al. 2008b).

The judicious investment in new satellite systems from many of the technologies illustrated above, where the proof-of-concept is well established would seem the way forward. In view of possible increases in the frequency of severe tropical cyclones due to a warming climate (Webster et al. 2005; Emanuel 2005; Elsner et al. 2008; Knutson et al. 2010) and the large population centers in vulnerable coastal areas, it is urgent that the community of scientists drive such progress, while not stifling development of new and innovative sensors.

Acknowledgments The authors thank members of Satellite Oceanography Laboratory, POI FEB Russian Academy of Science for Aqua AMSR-E, Terra and Aqua MODIS and Envisat ASAR processing. We are grateful to Professor Hans Graber for carrying out SAR image collection under the auspices of the Canadian "Hurricane Watch" program and for permission by Dr. Paris Vashon for use of the RADARSAT images in Sect. 2.3.

This work is partially supported by a grant from the Office of Naval Research, N0001411WX21223, from NSF grant ATM0631685 to University of Miami, and from the Russian Fund of Basic Research grant 11-05-ophi-m-2011.

References

- Adams, I.S., Hennon, C.C., Jones, L., Ahmad, K.A.: Evaluation of hurricane ocean vector winds from WindSat. *IEEE Trans. Geosci. Remote Sens.* **44**, 656–667 (2006)
- Adler, R.F., Huffman, G.J., Chang, A., Ferraro, R., Xie, P., Janowiak, J., Rudolf, B., Schneider, U., Curtis, S., Bolvin, D., Gruber, A., Susskind, J., Arkin, P.: The version 2 global precipitation climatology project (GPCP) monthly precipitation analysis (1979–present). *J Hydrometeor* **4**, 1147–1167 (2003)

- Alishouse, J.C., Snyder, S.A., Vongsathorn, J., Ferraro, R.R.: Determination of oceanic total column water vapour from the SSM/I. *IEEE Trans. Geosci. Remote Sens.* **28**, 811–816 (1990a)
- Alishouse, J.C., Snider, J.B., Westwater, E.R., Swift, C.T., Ruf, C.S., Snyder, S.A., Vongsathorn, J., Ferraro, R.R.: Determination of cloud liquid water-content using the SSM/I. *IEEE Trans. Geosci. Remote Sens.* **28**, 817–822 (1990b)
- Aziz, M.A., Raising, S.C., Asher, W.E., Rose, L.A., Gaiser, P.W., Horgan, K.A.: Effects of air–sea interaction parameters on ocean surface microwave emission at 10 and 37 GHz. *IEEE Trans. Geosci. Remote Sens.* **43**, 1763–1774 (2005)
- Baklanov, A.A., Grisogono, B., Bornstein, R., Mahrt, L., Zilitinkevich, S.S., Taylor, P., Larsen, S.E., Rotach, M.W., Fernando, H.J.S.: The nature, theory, and modeling of atmospheric planetary boundary layers. *Bul Amer Meteor Soc* **92**, 123–128 (2011)
- Basharinov, A.E., Gurvich, A.S., Egorov, S.T.: Radio Emission of the Earth as a Planet (Radioizluchenie Zemli kak Planeti). Nauka Publishing House, Moscow (1974). (188 pp., in Russian)
- Bell, W.: A preprocessor for SSMIS radiances scientific description. NWPSAF-MO-UD-014, Version 1.0. Met Office, United Kingdom: EUMETSAT (2006)
- Bennartz, R.: Optimal convolution of AMSU-B to AMSU-A. *J Atm. Oceanic Technol.* **17**, 1215–1225 (2000)
- Bentamy, A., Queffelec, P., Quilfen, Y., Katsaros, K.: Ocean surface wind fields estimated from satellite measurements. *IEEE Trans. Geosci. Remote Sens.* **37**, 2469–2486 (1999)
- Bentamy, A., Katsaros, K.B., Mestas-Núñez, A.M., Drennan, W.M., Forde, E.B., Roquet, H.: Satellite estimates of wind speed and latent heat flux over the global oceans. *J. Climate* **16**, 636–656 (2003)
- Bessho, K., DeMaria, M., Knaff, J.A.: Tropical cyclone wind retrievals from the advanced microwave sounder unit (AMSU): application to surface wind analysis. *J. Appl. Meteorol.* **45**, 399–415 (2006)
- Bettenhausen, M.H., Smith, C.K., Bevilacqua, R.M., Wang, N.-Y., Gaiser, P.W., Cox, S.: A nonlinear optimization algorithm for WindSat wind vector retrievals. *IEEE Trans. Geosci. Remote Sens.* **44**, 597–608 (2006)
- Black, P.G., Adams, W.L.: Guidance for estimating surface winds based on sea state observations from aircraft and sea state catalog. NOAA Tech. Memo. FCM-G1-1983, 83 pp (1983)
- Black, P.G., Swift, C.T.: Airborne stepped frequency microwave radiometer measurements of rainfall rate and surface wind speed in hurricanes. Preprints, Second Conf. on Radar Meteorology, Zurich, Switzerland, Amer Meteor Soc 433–438 (1984)
- Blackadar, A.K.: A single-layer theory of the vertical distribution of wind in a baroclinic neutral atmospheric boundary layer, Final Rept. AFCRL-65-531, Department of Meteorology, Pennsylvania State University, p. 22 (1965)
- Bobylev, L.P., Zabolotskikh, E.V., Mitnik, L.M., Mitnik, M.L.: Atmospheric water vapor and cloud liquid water retrieval over the Arctic Ocean using satellite passive microwave sensing. *IEEE Trans. Geosci. Remote Sens.* **49**, 283–294 (2010)
- Boukabara, S.A., Weng, F.: Microwave emissivity over ocean in all-weather conditions: validation using WINDSAT and airborne GPS dropsondes. *IEEE Trans. Geosci. Remote Sens.* **46**, 376–384 (2008)
- Buckreuss, S., Balzer, W., Muhlbauer, P., Werninghaus, R., Pitz, W.: The TerraSAR-X satellite project. *Proc IGARSS* **5**, 3096–3098 (2003)
- Businger, J.A., Wyngaard, J.C., Izumi, Y., Bradley, E.F.: Flux-profile relationships in the atmospheric surface layer. *J Atm. Sci.* **28**, 181–189 (1971)
- Campbell, A.B.: Radar Remote Sensing of Planetary Surfaces. Cambridge University Press, Cambridge (2002). (331 pp)
- Cardone, V.J.: Specification of the wind distribution in the marine boundary layer for wave forecasting. Report TR-69-01, Geophysical Sciences Laboratory. New York University. Available from NTIS #AD 702-490, 137 pp (1969)

- CCRS (2009) Tutorial: fundamentals of remote sensing, technical report, Canada Centre for Remote Sensing. <http://www.ccrs.nrcan.gc.ca/resource/tutor/gsa/red>
- Chen, S.H., Vandenbergh, F., Petty, G.W., Bresch, J.F.: Application of SSM/I satellite data to a hurricane simulation. *Q. J. Royal Meteorol. Soc.* **130**, 801–825 (2004). doi:[10.1256/qj.02.672004](https://doi.org/10.1256/qj.02.672004)
- Coletta, A., Angino, G., Battazza, F., Caltagirone, F., Impagnatiello, F., Valentini, G., Capuzi, A., Fagioli, S., Leonardi, R.: COSMO-SkyMed program: utilization and description of an advanced space EO dual-use asset. In: *Proceedings of Envisat Symposium*, 23–27 Apr 2007, ESA SP-636, Montreux, Switzerland (2007)
- Dagestad, K.-F., Johannessen, J.A., Hansen, M.W., Mouche, A., Collard, F.: Wind retrieval over the ocean from combined use of synthetic aperture radar and weather forecast models. In: *ESA Living Planet Symposium*, Bergen, Norway, 28 June–2 July. http://due.esrin.esa.int/stse/files/project/131-176-149-30_2010720123246.pdf (2010)
- Deardorff, J.W.: Parameterization of the planetary boundary layer for use in general circulation models. *Mon Wea Rev* **2**, 93–106 (1972)
- Demuth, J., DeMaria, M., Knaff, J.A., Vonder Haar, T.H.: Validation of an advanced microwave sounder unit (AMSU) tropical cyclone intensity and size estimation algorithm. *J Appl Meteor* **43**, 282–296 (2004)
- Demuth, J., DeMaria, M., Knaff, J.A.: Improvement of advanced microwave sounding unit tropical cyclone intensity and size estimation algorithms. *J. Appl. Climatol.* **45**, 1573–1581 (2006)
- Donelan, M.A., Haus, B.K., Reul, N., Plant, W.J., Stassnie, M., Graber, H.C., Brown, O.B., Satzman, E.S.: On the limiting aerodynamic roughness of the ocean in very strong winds. *Geophys. Res. Lett.* **31**, L18306 (2004)
- Dunion, J.P., Landsea, C.W., Houston, S.H., Powell, M.D.: A reanalysis of the surface winds for Hurricane Donna of 1960. *Mon. Weather Rev.* **131**, 1992–2011 (2003)
- Ebell, K., Löhnert, U., Crewell, S., Turner, D.D.: On characterizing the error in a remotely sensed liquid water content profile. *Atmos. Res.* **98**, 57–68 (2010)
- Ebuchi, N., Graber, H.C., Caruso, M.J.: Evaluation of wind vectors observed by QuikSCAT/SeaWinds using ocean buoy data. *J. Atmos. Oceanic Tech.* **19**, 2049–2062 (2002)
- Elsner, J., Kossin, P., Jagger, T.: The increasing intensity of the strongest tropical cyclones. *Nature* **455**, 92–95 (2008)
- El-Nimri, S.F., Linwood Jones, W., Uhlhorn, E., Ruf, C., Johnson, J., Black, P.: An improved C-band ocean surface emissivity model at hurricane-force wind speeds over a wide range of Earth incidence angles. *IEEE Geosci. Remote Sens. Lett.* **7**, 641–645 (2010)
- Emanuel, K.A.: Increasing destructiveness of tropical cyclones over the past 30 years. *Nature* **436**, 686–688 (2005)
- ESA (2002) ASAR Product Handbook, Technical report, European Space Agency, Paris, France
- Fairall, C.W., Bradley, E.F., Hare, J.E., Grachev, A.A., Edson, J.B.: Bulk parameterization of air-sea fluxes: updates and verification for the coare algorithm. *J. Climate* **19**, 571–591 (2003)
- Ferraro, R.R.: SSM/I derived global rainfall estimates for climatological purposes. *J. Geophys. Res.* **102**, 16715–16735 (1997)
- Ferraro, R.R., Weng, F., Grody, N.C., Zhao, L., Meng, H., Kongoli, C., Pellegrino, P., Qiu, S., Dean, C.: NOAA operational hydrological products derived from the advanced microwave sounding unit. *IEEE Trans. Geosci. Remote Sens.* **43**, 1036–1049 (2005)
- Franklin, J.L., Black, M.L., Valde, K.: GPS dropwindsonde wind profiles in hurricanes and their operational implications. *Wea. Forecast.* **18**, 32–44 (2003)
- Freilich, M.H., Dunbar, R.S.: *Seawinds: Algorithm Theoretical Basis Document*. Oregon State University Tech. Rep., Corvallis (2000). (Tech. Rep., 56 pp)
- Fu, L.L., Cazenave, A.: *Satellite Altimetry and Earth Sciences: A Handbook of Techniques and Applications*. Academic Press, San Diego (2001). (463 pp)
- Fu, L.L., Alsdorf, D., Rodriguez, E., Morrow, R., Mognard, N., Lambin, J., Vaze, P., Lafon, T.: The SWOT (Surface Water and Ocean Topography) Mission, OceansObs'09 white paper p. 17, available from <http://www.oceanobs09.net/> (2009)

- Gaiser, P.W., St Germain, K.M., Twarog, E.M., Poe, G.A., Purdy, W., Richardson, D., Grossman, W., Jones, W.L., Spencer, D., Golba, G., Cleveland, J., Choy, L., Bevilacqua, R.M., Chang, P.S.: The WindSat Spaceborne polarimetric microwave radiometer: sensor description and early orbit performance. *IEEE Trans. Geosci. Remote Sens.* **42**, 2347–2361 (2004)
- Gentemann, C.L., Meissner, T., Wentz, F.J.: Accuracy of satellite sea surface temperatures at 7 and 11 GHz. *IEEE Trans. Geosci. Remote Sens.* **48**, 1009–1018 (2010a). doi:[10.1109/TGRS.2009.2030322](https://doi.org/10.1109/TGRS.2009.2030322)
- Gentemann, C.L., Wentz, F.J., Brewer, M., Hilburn, K., Smith, D.: Passive microwave remote sensing of the ocean: an overview. In: Barale, V., Gower, J., Alberotanza, L. (eds.) *Oceanography from Space*, pp. 13–33. Springer, Heidelberg (2010b). (Revisited)
- Gentemann, C.L., Minnett, P.J., LeBorgne, P., Merchant, C.J.: Multi-satellite measurements of large diurnal SST warming events. *Geophys. Res. Lett.* **356**, L22602 (2008). doi:[10.1029/2008GL035730](https://doi.org/10.1029/2008GL035730)
- Gentemann, C.L., Minnett, P.J.: Radiometric measurements of ocean surface thermal variability. *J. Geophys. Res.* **113** (2008). doi:[10.1029/2007JC004540](https://doi.org/10.1029/2007JC004540)
- Goni, G., DeMaria, M., Knaff, J., Sapon, C., Ginnis, I., Bringas, F., Mavume, A., Lauer, C., Lin, I.-I., Ali, M., Sandery, P., Ramos-Buargue, S., Kang, K., Mehra, A., Chassignet, E., Halliwell, G.: Applications of satellite-derived ocean measurements to tropical cyclone intensity forecasting. *Oceanography* **22**, 190–197 (2009). doi:[10.5670/oceanog.2009.78](https://doi.org/10.5670/oceanog.2009.78)
- Goodberlet, M.A., Swift, C.T., Wilkerson, J.C.: Ocean surface wind speed measurements of the special sensor microwave/imager (SSM/I). *J. Geophys. Res.* **94**, 14547–14555 (1989)
- Goodberlet, M., Swift, C.T.: Development of a second generation stepped frequency microwave radiometer for IWRs. Tech. Rep. Prosensing, Inc. (formerly Quadrant Engineering), Amherst, MA, 42 pp (1996)
- Greenwald, T.J., Stephens, G.L., Vonder Haar, T.H., Jackson, D.L.: A physical retrieval of cloud liquid water over the global oceans using special sensor microwave/imager (SSM/I) observations. *J. Geophys. Res.* **98**, 18471–18488 (1993)
- Greenwald, T.J.: A 2-year comparison of AMSR-E and MODIS cloud liquid water path observations. *Geophys. Res. Lett.* **36**, L20805 (2009). doi:[10.1029/2009GL040394](https://doi.org/10.1029/2009GL040394)
- Grody, N.C., Zhao, J., Ferraro, R., Weng, F., Boers, R.: Determination of precipitable water and cloud liquid water from the NOAA 15 AMSU. *J. Geophys. Res.* **106**, 2943–2953 (2001)
- Harrington, R.F.: The development of a stepped frequency microwave radiometer and its application to remote sensing of the earth. NASA Technical Report, TM-81847, 169 pp (1980)
- Harper, B.A.: Tropical cyclone parameter estimation in the Australian Region, Systems Engineering Australia Pty Ltd for Woodside Energy Ltd, Perth, May 2002, 83 pp (2002)
- Hawkins, J.D., Lee, T.F., Turk, J., Sampson, C., Kent, J., Richardson, K.: Real-time Internet distribution of satellite products for tropical cyclone reconnaissance. *Bull. Amer. Meteor. Soc.* **82**, 567–578 (2001)
- Hawkins, J.D., Turk, F.J., Lee, T.F., Richardson, K.: Observations of tropical cyclones with the SSMIS. *IEEE Trans. Geosci. Remote Sens.* **46**, 901–912 (2008)
- Hock, T.F., Franklin, J.L.: The NCAR GPS dropwindsonde. *Bull. Amer. Meteor. Soc.* **80**, 407–420 (1999)
- Hollinger, J.P., Pierce, J.L., Poe, G.A.: SSM/I instrument evaluation. *IEEE Trans. Geosci. Remote Sens.* **28**, 781–790 (1990)
- Horstmann, J., Thompson, D.R., Monaldo, F., Graber, H.C., Iris, S.: Can synthetic aperture radars be used to estimate hurricane force winds? *Geophys. Res. Lett.* **32**, L22 801 (2005)
- Horváth, Á., Davies, R.: Comparison of microwave and optical cloud water path estimates from TMI, MODIS, and MISR. *J. Geophys. Res.* **112**, D01202 (2007). doi:[10.1029/2006JD007101](https://doi.org/10.1029/2006JD007101)
- Hurley, J.: Operational review: RADARSAT-1 & -2. SEA SAR 2010. 25–29 Jan 2010, ESA ESRIN, Frascati (Rome) Italy. (http://earth.eo.esa.int/workshops/seasar2010/8_Hurley.pdf) (2010)

- Imaoka, K., Kachi, M., Fujii, H., Murakami, H., Hori, M., Ono, A., Igarashi, T., Nakagawa, K., Oki, T., Honda, Y., Shimoda, H.: Global change observation mission (GCOM) for monitoring carbon, water cycles, and climate change. *Proc. IEEE* **98**, 717–734 (2010)
- Iris, S., Burger, G.: RADARSAT-1: Canadian space agency hurricane watch program. *Proc. IGARSS* **4**, 2742–2745 (2004)
- Jackson, C.R., Apel, J.R. (eds): Synthetic aperture radar (SAR) marine user's manual, NOAA NESDIS Office of Research and Applications, Washington DC. www.sarusersmanual.com (2004)
- Jones, W.L., Schroeder, L.C., Boggs, D.H., Bracalente, E.M., Browb, R.A., Dome, G.J., Pierson, W.J., Wentz, F.J.: The geophysical evaluation of remotely sensed wind vectors over the ocean. *J. Geophys. Res.* **87**, 3297–3317 (1982)
- Joyce, R.J., Janowiak, J.E., Arkin, P.A., Xie, P.: CMORPH: a method that produces global precipitation estimates from passive microwave and infrared data at high spatial and temporal resolution. *J. Hydromet.* **5**, 487–503 (2004)
- Jung, T., Ruprecht, E., Wagner, F.: Determination of cloud liquid water path over the oceans from SSM/I data using neural networks. *J. Appl. Meteor.* **37**, 832–844 (1998)
- Katsaros, K.B., Brown, R.A.: Legacy of the Seasat mission for studies of the atmosphere and air-sea-ice interactions. *Bull. Amer. Met. Soc.* **72**, 967–981 (1991)
- Katsaros, K.B., Forde, E.B., Chang, P., Liu, W.T.: QuikSCAT facilitates early detection of tropical depressions in 1999 hurricane season. *Geophys. Res. Lett.* **28**, 1043–1046 (2001)
- Katsaros, K.B., Bentamy, A., Bourassa, M., Ebuchi, N., Gower, J., Liu, W.T., Vignudelli, S.: Climate data Issues from an oceanographic remote sensing perspective. In: Tang, D. (ed.) *Remote Sensing of the Changing Oceans*. Springer, Berlin (2011). doi:[10.1007/978-642-16541-2_1](https://doi.org/10.1007/978-642-16541-2_1)
- Katsaros, K.B., Vachon, P., Black, P., Dodge, P., Uhlhorn, E.: Wind fields from SAR: could they improve our understanding of storm dynamics? *Johns Hopkins APL Tech. Dig.* **21**, 86–93 (2000)
- Kawanishi, T., Sezai, T., Ito, Y., Imaoka, K., Tukesima, T., Ishido, Y., Shibata, A., Miura, M., Inahata, H., Spencer, R.W.: The advanced microwave scanning radiometer for the earth observing system (AMSR-E), NASA's contribution to the EOS for global energy and water cycle studies. *IEEE Trans. Geosci. Remote Sens.* **41**, 184–194 (2003)
- Kidder, S.Q., Jones, A.S.: A blended satellite total precipitable water product for operational forecasting. *J. Atmos. Oceanic Technol.* **24**, 74–81 (2007)
- Kim, S.-W., Chung, E.-S., Yoon, S.-C., Sohn, B.-J., Sugimoto, N.: Intercomparisons of cloud-top and cloud-base heights from ground-based Lidar, CloudSat and CALIPSO measurements. *Int. J. Remote Sens.* **32**, 1179–1197 (2011)
- Knaff, J.A., Zehr, R.M., Goldberg, M.D., Kidder, S.Q.: An example of temperature structure differences in two cyclone systems derived from the advanced microwave sounding unit. *Wea. Forecast.* **15**, 476–483 (2000)
- Knaff, J.A., Zehr, R.M.: Reexamination of tropical cyclone pressure wind relationships. *Wea. Forecast.* **22**, 71–88 (2007)
- Knaff, J.A., DeMaria, M., Molenaar, D.A., Sampson, C.R., Seybold, M.G.: An automated, objective, multiple-satellite-platform tropical cyclone surface wind analysis. *J. Appl. Meteor. Climatol.* **50**, 2149–2166 (2011)
- Knutson, T., McBride, L., Chan, C., Emanuel, K., Holland, G., Landsea, C., Held, I., Kossin, J., Srivastava, A., Sugi, M.: Tropical cyclones and climate change. *Nat. Geosci.* **3**, 157–163 (2010)
- Kossin, J.P., Schubert, W.H.: Mesovortices, polygonal flow patterns, and rapid pressure falls in hurricane-like vortices. *J. Atmos. Sci.* **58**, 2196–2209 (2001)
- Kossin, J.P., McNoldy, B.D., Schubert, W.H.: Vortical swirls in hurricane eye clouds. *Mon. Weather. Rev.* **130**, 3144–3149 (2002)
- Kossin, J.P., Schubert, W.H.: Mesovortices in Hurricane Isabel (2003). *Bull. Amer. Meteor. Soc.* **85**, 151–153 (2004)

- Kramer, H.J.: Observation of the Earth and Its Environment. Survey of Missions and Sensors. 4th edn. Springer, Berlin (2002). ISBN 3-540-42388-5, XXIX + 1510 pp., 1 CD-ROM
- Krasnopolsky, V.M., Gemmill, W.H., Breaker, L.C.: A neural network multiparameter algorithm for SSM/I ocean retrievals—comparisons and validations. *Remote Sens. Environ.* **73**, 133–142 (2000)
- Kummerow, C., Barnes, W., Kozu, T., Shiue, J., Simpson, J.: The tropical rainfall measuring mission (TRMM) sensor package. *J. Atmos. Oceanic Technol.* **15**, 808–816 (1998)
- Kummerow, C., et al.: The status of the tropical rainfall measuring mission (TRMM) after two years in orbit. *J. Appl. Meteor.* **39**, 1965–1982 (2000)
- Kunkee, D.B., Poe, G.A., Boucher, D.J., Swadley, S.D., Hong, Y., Wessel, J.E., Uliana, E.A.: Design and evaluation of the first special sensor microwave imager/sounder. *IEEE Trans. Geosci. Remote Sens.* **46**, 863–883 (2008)
- L'Ecuyer, T.S., Jiang, J.H.: Touring the atmosphere aboard the A-train. *Phys. Today* **7**, 36–41 (2010)
- Lee, T.F., Bankert, R.L., Mitrescu, C.: Meteorological education and training using A-train profilers. *Bull. Amer. Meteorol. Soc.* **93**, 687–696 (2012)
- Lee, T.F., Nelson, C.S., Dills, P., Riishojgaard, L.P., Jones, A., Li, L., Miller, S., Flynn, L.E., Jedlovec, G., McCarty, W., Hoffman, C., McWilliams, G.: NPOESS: next-generation operational global earth observations. *Bull. Amer. Meteorol. Soc.* **91**, 727–740 (2010)
- Lehner, S., He, M.-X., Li, X.-M., Velotto D., Ren Y.-Z. Application of coastal monitoring using high resolution SAR. 2011 Dragon 2 Symposium, Praga Czech Republic, 20–24 June (2011)
- Lin, I.-I., Wu, C.C., Pun, I.-P.: Upper ocean thermal structure and the western North Pacific category 5 typhoons. Part I. Ocean features and category 5 typhoons' intensification. *Mon. Weather Rev.* **136**, 288–306 (2008)
- Liu, G.-R., Chao, C.C., Ho, C.-Y.: Applying satellite-estimated storm rotation speed to improve typhoon rainfall potential technique. *Wea. Forecast.* **23**, 259–269 (2008a)
- Liu, G., Curry, J.A.: Determination of characteristic feature of cloud liquid water from satellite microwave measurements. *J. Geophys. Res.* **98**, 5069–5092 (1993)
- Liu, W.T., Tang, W.: Equivalent Neutral Wind. JPL Publication 96-17, JetPropulsion Laboratory, Pasadena, 16 pp. <http://airsea.jpl.nasa.gov/publication/paper/Liu-Tang-1996-jpl.pdf> (1996)
- Liu, W.T., Xie, X.: Ocean-atmosphere momentum coupling in the Kuroshio extension observed from space. *J. Oceanogr.* **64**, 631–637 (2008)
- Liu, W.T., Tang, W., Xie, X., Naval Gund, R.R., Xu, K.: Power density of ocean surface wind from international scatterometers tandem missions. *Int. J. Remote Sens.* **29**, 6109–6116 (2008b)
- Liu, Q., Weng, F., English, S.J.: An improved fast microwave water emissivity model. *IEEE Trans. Geosci. Remote Sens.* **49**, 1238–1250 (2011)
- Lonfat, M., Marks, F.D., Chen, S.S.: Precipitation distribution in tropical cyclones using the tropical rainfall measuring mission (TRMM) microwave imager: a global perspective. *Mon. Weather Rev.* **132**, 1645–1660 (2004)
- Long, D.G.: Reconstruction of high resolution ocean wind vectors from low resolution scatterometer measurements. *Proc. SPIE* vol. 5562 Image Reconstruction from Incomplete Data III, Bellingham, WA, SPIE, 196–207 (2004)
- Mainelli, M., DeMaria, M., Shay, L.K., Goni, G.: Application of oceanic heat content estimation to operational forecasting of recent Atlantic category 5 Hurricanes. *Wea. Forecast.* **23**, 1–16 (2008)
- Mallet, C., Moreau, E., Casagrande, L., Klapisz, C.: Determination of integrated cloud liquid water path and total precipitate water from SSM/I data using a neural network algorithm. *Int. J. Remote Sens.* **23**, 661–674 (2002)
- Matrosov, S.Y.: CloudSat studies of stratiform precipitation systems observed in the vicinity of the Southern Great Plains atmospheric radiation measurement site. *J. Appl. Meteor. Clim.* **49**, 1756–1765 (2010)

- Mätzler, C., Rosenkranz, P.W., Cermak, J.: Microwave absorption of supercooled clouds and implications for the dielectric properties of water. *J. Geophys. Res.* **115**, D23208 (2010). doi:[10.1029/2010JD014283](https://doi.org/10.1029/2010JD014283)
- Meissner, T., Wentz, F.J.: Ocean retrievals for WindSat: radiative transfer model, algorithm, validation. In: 9th Specialist Meeting Microwave Radiometry Remote Sensing Applications, Puerto Rico, USA, 2006. Available: [http://www.remss.com/papers/meissner_and_wentz\(2006\).pdf](http://www.remss.com/papers/meissner_and_wentz(2006).pdf) (2006)
- Meissner, T., Wentz, F.J.: Wind retrievals under rain for passive satellite microwave radiometers and its application to hurricane tracking. *Proc. IGARSS* (2008)
- Miller, B.I.: The three-dimensional wind structure around a tropical cyclone. National Hurricane Research Project Rept. 15, U.S. Weather Bureau, 41 pp (1958)
- Mims, A., Kroodsma, R., Ruf, C., McKague, D.: WindSat retrieval of ocean surface wind speed in tropical cyclones. In: *Proceedings of IGARSS 2010*. Hawaii, USA, pp. 1831–1834, 26–30 July 2010
- Mitnik, L. M.: Algorithm for atmospheric total water vapor determination from satellite measurements of microwave radiometric emission *Proc. USSR Hydrometeorological Cent.* **50**, 94–102 (1969) (in Russian)
- Mitnik, L. M.: Cloud investigation by microwave radiometric technique. RIHMI-WDC, Obninsk, 67 pp (1978) (in Russian)
- Mitnik, L.M., Mitnik, M.L.: Retrieval of atmospheric and ocean surface parameters from ADEOS-II AMSR data: comparison of errors of global and regional algorithms. *Radio Sci.* **38**, 8065 (2003). doi:[10.1029/2002RS002659](https://doi.org/10.1029/2002RS002659)
- Mitnik, L.M., Mitnik, M.L.: Retrieval of total water vapor content and total cloud liquid water content over the ocean by microwave sensing from DMSP, TRMM, AQUA and ADEOS-II satellites. *Inv. Earth Space* **4**, 34–41 (2006). (in Russian)
- Mitnik, L.M., Mitnik, M.L.: AMSR-E advanced wind speed retrieval algorithm and its application to marine weather systems. In: *Proceedings of IGARSS 2010*, Hawaii, pp. 3224–3227, 26–30 July 2010
- Mitnik, M.L., Mitnik, L.M.: Retrieval algorithm of sea surface wind speed from AMSR-E microwave radiometer data and its application to weather system analysis in tropical zone. *Curr. Probl. Earth Remote Sens. Space* **8**, 297–303 (2011). (in Russian)
- Mitnik, L., Chen, K.-S., Wang, J.-T., Mitnik, M., Hsu, M.-K.: Satellite microwave observations of typhoon Herb (1996) near Taiwan. *Glob. Atmos. Ocean Syst.* **8**, 19–39 (2002)
- Mitnik, L.M., Mitnik, M.L., Gurvich, I.A.: Monitoring tropical cyclone evolution over the NW Pacific with Aqua AMSR-E and Envisat ASAR. In: *Proceedings of 31st International Symposium Remote Sensing Environment (ISRSE)*. St. Petersburg, 20–24 June 2005. <http://www.isprs.org/publications/related/ISRSE/html/papers/376.pdf> (2005a)
- Mitnik, M.L., Mitnik, L.M.: Oxygen channels of ADEOS-II AMSR: comparison of the measured and simulated brightness temperatures. In: *Proceedings of 31st ISRSE*, St. Petersburg. <http://www.isprs.org/publications/related/ISRSE/html/papers/908.pdf> (2005b)
- Mitnik, L.M., Mitnik, M.L., Zabolotskikh, E.V.: Microwave sensing of the atmosphere-ocean system with ADEOS-II AMSR and Aqua AMSR-E. *J. Remote Sens. Soc. Japan* **29**, 156–165 (2009)
- Mitrescu, C., L'Ecuyer, T., Haynes, J., Miller, S., Turk, J.: CloudSat precipitation profiling algorithm—model description. *J. Appl. Meteor. Climatol.* **49**, 991–1003 (2010)
- Montgomery, M.T., Vladimirov, V.A., Denissenko, P.V.: An experimental study on hurricane mesovortices. *J. Fluid Mech.* **471**, 1–32 (2002)
- Moreau, E., Mallet, C., Maxbboux, B., Badran, F., Klapisz, C.: Atmospheric liquid water retrieval using a gated experts neural network. *J. Atmos. Ocean Technol.* **19**, 457–467 (2002)
- Morena, L.C., James, K., Beck, J.: An introduction to the RADARSAT-2 mission. *Canadian J. Remote Sens.* **30**, 221–234 (2004)
- Njoku, E.G.: Passive microwave remote sensing of the earth from space—a review. *Proc. IEEE* **70**, 728–750 (1982). doi:[10.1109/PROC.1982.12380](https://doi.org/10.1109/PROC.1982.12380)

- Nordberg, W., Conaway, J., Thaddeus, P.: Microwave observations of the sea state from aircraft. *Q. J. Royal Meteorol. Soc.* **95**, 408–413 (1969)
- O'Dell, C.W., Wentz, F.J., Bennartz, R.: Cloud liquid water path from satellite-based passive microwave observations: a new climatology over the global oceans. *J. Climate* **21**, 1721–1739 (2008)
- Oki, T., Imaoka, K., Kachi, M.: AMSR instrument on GCOM-W1/2: concepts and applications. In: *Proceedings of IGARSS 2010 Honolulu*, pp. 1363–1366, 25–30 July 2010
- Petty, G.W., Katsaros, K.B.: The response of the SSM/I to the marine environment. Part I: An analytic model for the atmospheric component of observed brightness temperatures. *J. Atmos. Oceanic Technol.* **9**, 746–761 (1992)
- Pielke, R.A., Landsea, C.W.: Normalized hurricane damages in the United States, 1923–1995. *Wea. Forecast.* **13**, 621–631 (1998)
- Poe, G., St. Germain, K., Bobak, J., et al.: DMSP calibration/validation plan for the special sensor microwave imager sounder (SSMIS). Naval Research Laboratory, Washington, DC, USA (2001)
- Powell, M.D.: Evaluations of diagnostic marine boundary-layer models applied to hurricanes. *Mon. Weather Rev.* **108**, 57–766 (1980)
- Powell, M.D., Houston, S.H., Reinhold, T.A.: Hurricane Andrew's landfall in south Florida. Part I: Standardizing measurements for documentation of surface wind fields. *Wea. Forecast.* **11**, 304–328 (1996)
- Powell, M.D., Black, P.G., Houston, S.H., Reinhold, T.A.: GPS sonde insights on boundary layer structure in hurricanes. In: *Preprints, 23rd Conference on Hurricanes and Tropical Meteorology*, Dallas, TX, American Meteorol. Soc. Boston, pp. 881–884, 10–15 Jan 1999
- Powell, M.D., Vickery, P.J., Reinhold, T.A.: Reduced drag coefficient for high wind speeds in tropical cyclones. *Nature* **422**, 279–283 (2003)
- Prasad, A.K., Singh, R.P.: Features of hurricane Katrina using multi sensor data. *Intern. J. Remote Sens.* **28**, 4709–4713 (2007). doi:[10.1080/01431160500522668](https://doi.org/10.1080/01431160500522668)
- Quilfen, Y., Chapron, B., Tournadre, J.: Satellite microwave surface observations in tropical cyclones. *Mon. Weather Rev.* **138**, 421–437 (2010). doi:<http://dx.doi.org/10.1175/2009MWR3040.1>
- Quilfen, Y., Vandemark, D., Chapron, B., Feng, H., Sienkiewicz, J.: Estimating gale to hurricane force winds using the satellite altimeter. *J. Atm. Oceanic Technol.* **28**, 453–458 (2011)
- Reynolds, R.W., Gentemann, C.L., Corlett, G.K.: Evaluation of AATSR and TMI satellite SST data. *J. Climate* **23**, 152–165 (2010). doi:[10.1175/2009JCL132421](https://doi.org/10.1175/2009JCL132421)
- Reppucci, A., Lehner, S., Schulz-Stellenfleth, J., Brusch, S.: Tropical cyclone intensity estimated from wide-swath SAR images. *IEEE Trans. Geosci. Remote Sens.* **48**, 1639–1649 (2010)
- Reynolds, R.W., Smith, T.M., Liu, C., Chelton, D.B., Casey, K.S., Schlax, M.G.: Daily high-resolution-blended analyses for sea surface temperature. *J. Climate* **20**, 5473–5496 (2007)
- Ross, D.B., Cardone, V.: Observations of oceanic whitecaps and their relation to remote measurements of surface wind speed. *J. Geophys. Res.* **79**, 444–452 (1974)
- Robinson, I.S.: *Measuring the Oceans from Space: Theoretical Principles and Methods of Satellite Oceanography*. Springer, Berlin (2004). (646 p)
- Sasaki, Y., Asanuma, I., Muneyama, K., Naito, G., Suzuki, T.: The dependence of sea surface microwave emission on wind speed, frequency, incidence angle, and polarization over the frequency range from 1 to 40 GHz. *IEEE Trans. Geosci. Remote Sens.* **25**, 138–146 (1987)
- Schubert, W.H., Montgomery, M.T., Taft, R.K., Guinn, T.A., Fulton, S.R., Kossin, J.P., Edwards, J.P.: Polygonal eyewalls, asymmetric eye contraction and potential vorticity mixing in hurricanes. *J. Atmos. Sci.* **56**, 1197–1223 (1999)
- Shi, W., Wang, M.: Observations of a hurricane Katrina-induced phytoplankton bloom in the Gulf of Mexico. *Geophys. Res. Lett.* **34**, L11607 (2007). doi:[10.1029/2007GL02972](https://doi.org/10.1029/2007GL02972)
- Shibata, A.: AMSR/AMSR-E SST algorithm developments; removal of ocean wind effect. *Italian J. Remote Sensing*, **30/31**, 131–142 (2004)

- Shibata, A.: A wind speed retrieval algorithm by combining 6 and 10 GHz data from advanced microwave scanning radiometer: wind speed inside hurricanes. *J. Oceanogr.* **62**, 351–359 (2006)
- Shibata, A.: Algorithm development in retrieving sea surface temperature and sea surface wind speed. *J. Remote Sens. Soc. Japan* **29**, 167–173 (2009)
- Simpson, J., Adler, R.F., North, G.R.: Proposed tropical rainfall measuring mission (TRMM) satellite. *Bull. Amer. Meteor. Soc.* **69**, 278–295 (1988)
- Smith, C.K., Bettenhausen, M., Gaiser, P.W.: A statistical approach to WindSat ocean surface wind vector retrieval. *IEEE Geosci. Remote Sens. Lett.* **3**, 164–168 (2006)
- Spencer, R.W., Braswell, W.D.: Atlantic tropical cyclone monitoring with AMSU-A: estimation of maximum sustained wind speeds. *Mon. Weather Rev.* **129**, 1518–1532 (2001). doi:[10.1175/1520-0493\(2001\)129<1518:ATCMWA>2.0.CO;2](https://doi.org/10.1175/1520-0493(2001)129<1518:ATCMWA>2.0.CO;2)
- Staelin, D.H., Chen, F.W.: Precipitation observations near 54 and 183 GHz using the NOAA-15 satellite. *IEEE Trans. Geosci. Remote Sens.* **38**, 2322–2332 (2000)
- Stephens, G.L., Vane, D.G., Boain, R.J., Mace, G.G., Sassen, K., Wang, Z., Illingworth, A.J., O'Connor, E.J., Rossow, W.B., Durden, S.L., Miller, S.D., Austin, R.T., Benedetti, A., Mitrescu, C., the CloudSat Science Team: The CloudSat mission and the A-train. *Bull. Am. Meteorol. Soc.* **83**, 1771–1790 (2002)
- Stephens, G.L., Kummerow, C.D.: The remote sensing of clouds and precipitation from space: a review. *J. Atmos. Sci.* **64**, 3742–3765 (2007)
- St. Germain, K.M., Swift, C.T., Grenfell, T.C.: Determination of dielectric constant of young sea ice using microwave spectral radiometry. *J. Geophys. Res.* **98**, 4675–4679 (1993)
- Stoffelen, A.: A simple method for calibration of a scatterometer over the ocean. *J. Atmosph. Oceanic Technol.* **16**, 275–282 (1999)
- Surussavadee, C., Staelin, D.H.: NPOESS precipitation retrievals using the ATMS passive microwave spectrometer. In: *Proceedings of IGARSS 2008*, Boston, MA, IEEE, vol. 5, pp. 570–573 (2008)
- Swift, C.T., Goodberlet, M.A.: Passive microwave remote sensing of the ocean. *Specialist Meeting on Microwave Radiometry and Remote Sensing Applications*. Boulder, CO, U.S. DOC/NOAA/ERL/WPL, pp. 87–93 (1992)
- Swift, C.T., Dehority, D.C., Tanner, A.B., McIntosh, R.E.: Passive microwave spectral emission from saline ice at C-band during the growth phase. *IEEE Trans. Geosci. Remote Sens.* **GE-24**, 840–848 (1986)
- Tanelli, S., Durden, S.L., Pak, K.S., Reinke, D.G., Partain, P., Haynes, J.M., Marchand, R.T.: CloudSat's cloud profiling radar after two years in orbit: performance, calibration, and processing. *IEEE Trans. Geosci. Remote Sens.* **46**, 3560–3573 (2008)
- Tanner, A.C., Swift, C.T., Black, P.G.: Operational airborne remote sensing of wind speeds in hurricanes. In: *Preprints, 17th Conference on Hurricanes and Tropical Meteorology*, Miami, FL, American Meteor. Society, pp. 385–387 (1987)
- Turner, D.D., Cadeddu, M.P., Löhnert, U., Crewell, S., Vogelmann, A.M.: Modifications to the water vapor continuum in the microwave suggested by ground-based 150-GHz observations. *IEEE Trans. Geosci. Remote Sens.* **47**, 3326–3337 (2009)
- Uhlhorn, E.W., Black, P.G.: Verification of remotely sensed sea surface winds in hurricanes. *J. Atmos. Oceanic Technol.* **20**, 99–116 (2003)
- Uhlhorn, E.W., Black, P.G., Franklin, J.L., Goodberlet, M., Carswell, J., Goldstein, A.S.: Hurricane surface wind measurements from an operational stepped frequency microwave radiometer. *Mon. Weather Rev.* **135**, 3070–3085 (2007)
- Vachon, P.W., Katsaros, K.B.: Atmospheric cyclones from spaceborne SAR. *Backscatter* **10**, 14–19 (1999)
- Vachon, P.W., Black, P.G., Dodge, P.P., Katsaros, K.B., Clemente-Colon, P., Pichel, W., McDonnell, K.: RADARSAT-1 Hurricane watch. In: *Proceedings of IGARSS 2001*, Sydney, Australia, 9–13 July 2001, on CD-ROM, 3 p
- Valenzuela, G.: Theories for the interaction of electromagnetic and oceanic waves—a review. *Bound Layer Meteorol* **13**, 61–85 (1978)

- Vignudelli, S., et al.: Satellite altimetry: sailing closer to the coast. In: Tang D. (ed.) Remote Sensing of the Changing Oceans, Springer, Berlin (2011). doi:[10.1007/978-3-16541-2_11](https://doi.org/10.1007/978-3-16541-2_11)
- Webster, P.J., Holland, G.J., Curry, J.A., Chang, H.R.: Changes in tropical cyclone number, duration, and intensity in a warming environment. *Science* **309**, 1844–1846 (2005)
- Webster, W.J., Wilheit, T.T., Ross, D.B., Gloersen, P.: Spectral characteristics of the microwave emission from a wind-driven foam covered sea. *J. Geophys. Res.* **81**, 3095–3099 (1976a)
- Weng, F., Grody, N.C.: Retrieval of cloud liquid water using the special sensor microwave imager (SSM/I). *J. Geophys. Res.* **99**, 25535–25551 (1994)
- Weng, F., Zhao, L., Poe, G., Ferraro, R., Li, X., Grody, N.: AMSU cloud and precipitation algorithms. *Radio Sci.* **38**, 8068–8079 (2003)
- Weng, F., Grody, N.C., Ferraro, R.R., Basist, A., Forsyth, D.: Cloud liquid water climatology derived from the special sensor microwave imager. *J. Climate* **10**, 1086–1098 (1997)
- Weng, F., Zhu, T., Yan, B.: Satellite data assimilation in numerical weather prediction models. Part II: Uses of rain-affected radiances from microwave observations for hurricane vortex analysis. *J. Atm. Sci.* **64**, 3910–3925 (2007)
- Wentz, F.J.: A model function for ocean microwave brightness temperatures. *J. Geophys. Res.* **88**, 1892–1908 (1983)
- Wentz, F.J., Mattox, L.A., Peteherych, S.: New algorithms for microwave measurements of ocean winds: applications to SEASAT and the special sensor microwave imager. *J. Geophys. Res.* **91**, 2289–2307 (1986)
- Wentz, F.J., Spencer, R.W.: SSM/I rain retrievals within a unified all-weather ocean algorithm. *J. Atm. Sci.* **55**, 1613–1627 (1998)
- Wentz, F.J.: A well-calibrated ocean algorithm for special sensor microwave/imager. *J. Geophys. Res.* **102**, 8703–8718 (1997)
- Wentz, F.J.: Advanced algorithms for QuikScat and SeaWinds/AMSR. In: Proceedings of IGARSS 2001 Sydney, Australia (2001)
- Wentz, F.J., Gentemann, C., Smith, D., Chelton, D.: Satellite measurements of sea surface temperature through clouds. *Science* **288**, 847–850 (2000)
- Wentz, F. J., Smith, D. K., Mears, C. A., Gentemann, C. L.: Advanced algorithms for QuikScat and SeaWinds/AMSR. In: Proceedings of Geoscience and Remote Sensing Symposium, 2001. IGARSS '01. IEEE 2001 International, **3** (2001). doi:[10.1109/IGARSS.2001.976752](https://doi.org/10.1109/IGARSS.2001.976752)
- Wilheit, T., Kummerow, C., Ferraro, R.: Rainfall algorithms for AMSR-E. *IEEE Trans. Geosci. Remote Sens.* **41**, 204–214 (2003)
- Wilheit, T.T.: A model for the microwave emissivity of the ocean's surface. *IEEE Trans. Geosci. Electron.* **GE-17**, 244–249 (1979)
- Wimmers, A.J., Velden, C.S.: MIMIC: a new approach to visualizing satellite microwave imagery of tropical cyclones. *Bull. Amer. Meteor. Soc.* **88**, 1187–1196 (2007)
- Woiceshyn, P., Wurtele, M., Boggs, D., McGoldrick, L., Peteherych, S.: The necessity for a new parameterization of an empirical model for wind/ocean scatterometry. *J. Geophys. Res.* **91**, 2273–2288 (1986)
- Yan, B., Weng, F.: Applications of AMSR-E measurements for tropical cyclone predictions, part I: retrieval of sea surface temperature and wind speed. *Adv. Atm. Sci.* **25**, 227–245 (2008)
- Yueh, S.H., Wilson, W., Dinardo, S., Hsiao, S.V.: Polarimetric microwave wind radiometer model function and retrieval testing for WindSat. *IEEE Trans. Geosci. Remote Sens.* **44**, 584–596 (2006)
- Zecchetto, S.: Ocean wind fields from satellite active microwave sensors. In: Imperatore, P., Riccio, D. (eds.) *Geoscience and Remote Sensing, New Achievements*. Intech, pp. 263–283 (2010)

Typhoon Impact and Crisis Management

Tang, D.L.; Sui, G. (Eds.)

2014, XXIII, 578 p. 198 illus., 158 illus. in color.,

Hardcover

ISBN: 978-3-642-40694-2